Dynamical evaluation of ocean models using the Gulf Stream as an example

Harley E. Hurlburt[1], E. Joseph Metzger[1], James G. Richman[1], Eric P. Chassignet[2], Yann Drillet[3], Matthew W. Hecht[4], Olivier Le Galloudec[3], Xiaobiao Xu[5], and Luis Zamudio[2]

[1]Oceanography Division, Naval Research Laboratory, Stennis Space Center, MS USA

[2]Center for Ocean-Atmospheric Prediction Studies (COAPS), Florida State University, Tallahassee, FL USA

[3]Mercator Océan, Ramonville-Saint-Agne, France

[4]Computational Physics Group, CCS Division, Los Alamos National Laboratory, Los Alamos, NM USA

[5]Department of Marine Science, University of Southern Mississippi, Stennis Space Center, MS USA

1. Introduction

Ocean models run with atmospheric forcing but without ocean data assimilation are useful in studies of ocean model dynamics and simulation skill. Models that give realistic simulations with accurate dynamics, when run without data assimilation, are essential for eddy-resolving ocean prediction because of the multiple roles that ocean models must play in ocean nowcasting and forecasting, including dynamical interpolation during data assimilation, representing sparsely observed subsurface ocean features from the mixed layer depth to abyssal currents, converting atmospheric forcing into ocean responses, imposing topographic and geometric constraints, performing ocean forecasts, and providing boundary and initial conditions to nested regional and coastal models. A wide range of ocean dynamics contribute to these different roles. Here we focus on evaluating the dynamics of mid-latitude ocean currents simulated by state-of-the-art, eddy-resolving ocean general circulation models (OGCMs) with high vertical resolution, using the Gulf Stream as an example.

Dynamical evaluation of current systems simulated by OGCMs has been a challenge because of the complexity of the models and the current systems, a topic discussed in recent reviews by Chassignet and Marshall (2008) and Hecht and Smith (2008) in relation to the Gulf Stream and North Atlantic. In some regions more substantial progress has been made. Tsujino et al. (2006) investigated the dynamics of large amplitude Kuroshio meanders south of Japan. Usui et al. (2006) used the same model to make Kuroshio forecasts from a data-assimilative initial state, typically demonstrating 40 to 60-day forecast skill south of Japan. Usui et al. (2008a,b) also used the model in dynamical studies of a 1993-2004 data-assimilative hindcast. Hurlburt et al. (2008b) examined OGCM dynamics and their relation to the underlying topography in studying mean Kuroshio meanders east of Japan and mean currents in the southern

Report Documentation Page

Form Approved
OMB No. 0704-0188

1. REPORT DATE	2. REPORT TYPE	3. DATES COVERED
JAN 2010		**00-00-2010 to 00-00-2010**

4. TITLE AND SUBTITLE	5a. CONTRACT NUMBER
Dynamical evaluation of ocean models using the Gulf Stream as an example	5b. GRANT NUMBER
	5c. PROGRAM ELEMENT NUMBER
6. AUTHOR(S)	5d. PROJECT NUMBER
	5e. TASK NUMBER
	5f. WORK UNIT NUMBER
7. PERFORMING ORGANIZATION NAME(S) AND ADDRESS(ES) **Naval Research Laboratory,Oceanography Division,Stennis Space Center,MS,39529-5004**	8. PERFORMING ORGANIZATION REPORT NUMBER
9. SPONSORING/MONITORING AGENCY NAME(S) AND ADDRESS(ES)	10. SPONSOR/MONITOR'S ACRONYM(S)
	11. SPONSOR/MONITOR'S REPORT NUMBER(S)

12. DISTRIBUTION/AVAILABILITY STATEMENT
Approved for public release; distribution unlimited

13. SUPPLEMENTARY NOTES
GODAE Summer School 11-22 January 2010, Perth Australia

14. ABSTRACT

15. SUBJECT TERMS

16. SECURITY CLASSIFICATION OF:			17. LIMITATION OF ABSTRACT	18. NUMBER OF PAGES	19a. NAME OF RESPONSIBLE PERSON
a. REPORT **unclassified**	b. ABSTRACT **unclassified**	c. THIS PAGE **unclassified**	**Same as Report (SAR)**	**44**	

half of the Japan/East Sea. The simulations were consistent with observations and with dynamics found in purely hydrodynamic models with lower vertical resolution and vertically-compressed but otherwise realistic topography confined to the lowest layer. The same Japan/East Sea OGCM simulation modeled the dynamics of intrathermocline eddy formation in that region in agreement with observations, as discussed in Hogan and Hurlburt (2006). The intrathermocline nature of some Japan/East Sea eddies could not be simulated by the purely hydrodynamic model. Hurlburt et al. (2008b) also investigated OGCM dynamics in simulating the Southland Current system east of South Island, New Zealand, where the topography of the Campbell Plateau and the Chatham Rise intrude well into the stratified ocean so that the design of the low vertical resolution model did not apply. In this case an alternative approach was used to investigate the dynamics. Recent observational evidence was sufficient to provide strong support for the results of the study and to discredit an earlier theory.

In dynamical evaluation of the Gulf Stream simulations by eddy-resolving global and basin-scale OGCMs, we adopt an augmented version of the approach used by Hurlburt et al. (2008b) for OGCM simulations of the Kuroshio and Japan/East Sea. Thus we build from an explanation of Gulf Stream separation from a western boundary and its pathway to the east in Hurlburt and Hogan (2008). This explanation was derived using results from a 5-layer hydrodynamic model with vertically-compressed but otherwise realistic topography confined to the lowest layer. It was tested versus observational evidence and theory, parts of the latter contributing directly to the explanation. In Section 2 we discuss the explanation and related 5-layer model results, theory, and observational evidence. In Section 3 we evaluate Gulf Stream dynamics in eddy-resolving OGCM simulations by the HYbrid Coordinate Ocean Model (HYCOM) (Bleck, 2002), the Miami Isopycnic Coordinate Ocean Model (MICOM) (Bleck and Smith, 1990), the Nucleus for European Modelling of the Ocean (NEMO) (Madec, 2008) as used in the French Mercator ocean prediction effort, and the Parallel Ocean Program (POP) (Smith et al. 2000). Both simulations with a realistic Gulf Stream and those with a variety of unrealistic features are assessed and specific deficiencies are identified. In Section 4 we assess the impacts of data assimilation on variables relevant to Gulf Stream dynamics that are sparsely observed, in some cases not observed at all in real time. Are realistic model dynamics maintained in data-assimilative models? Are unrealistic dynamics improved? What are the impacts of dynamics on Gulf Stream forecast skill?

2. Dynamics of Gulf Stream boundary separation and its pathway to the east

2.1 Linear model simulation of the Gulf Stream

As an initial step, we examine a linear barotropic solution with the same wind forcing and upper ocean transport for the Atlantic meridional overturning circulation (AMOC) as the

nonlinear solutions discussed in Section 2. The model boundary is located at the shelf break and the resolution is comparable to that used in nonlinear solutions discussed later in this section. The spun up mean solution has a Sverdrup (1947) interior, Munk (1950) western boundary currents and is consistent with the Godfrey (1989) island rule, except that, unlike Munk (1950), the solution is obtained by running a numerical model with horizontal friction applied everywhere.

Figure 1 depicts the mass transport streamfunction from a 1/16º l.5 layer linear simulation forced by the smoothed Hellerman and Rosenstein (1983) wind stress climatology plus the northward upper ocean flow of a 14 Sv AMOC. In comparison to the overlaid mean IR northwall pathway that lies along the northern edge of the Gulf Stream, the linear solution gives two unrealistic pathways, a broad one centered near the observed separation latitude (35.5ºN) that extends eastward and a second one with nearly the same transport extending northward along the western boundary. The eastward pathway is wind-driven (~22 Sv) and the northward pathway has a 14 Sv AMOC component plus an 8 Sv wind-driven component, but both pathways contribute to a situation where ~31 Sv out of 44 Sv (~70%) separate from the western boundary north of the observed separation latitude. From Figure 1 it is easy to appreciate the challenge of simulating an accurate nonlinear Gulf Stream pathway in an ocean model. See Townsend et al. (2000) for linear solutions from 11 different wind stress climatologies.

2.2 Impacts of the eddy-driven abyssal circulation and the Deep Western Boundary Current (DWBC) on Gulf Stream boundary separation and its pathway to the east

It has been a popular theory, proposed by Thompson and Schmitz (1989), that the DWBC affects Gulf Stream separation from the western boundary as it passes underneath at the separation point. To investigate this hypothesis Hurlburt and Hogan (2008) used a nonlinear 5-layer hydrodynamic model covering the same domain shown in Figure 1. They also used the same monthly climatological wind forcing and included a 14 Sv AMOC, the latter via inflow and outflow ports in the northern and southern boundaries. The northward upper ocean component of the AMOC resides in the top 4 layers and was always included, while the DWBC residing in the abyssal layer was included in the simulations in the left column of Figure 2 and turned off in the simulations in the right column. Since the model was purely hydrodynamic, the DWBC could be turned off without altering the watermass characteristics. In the three rows of Figure 2 the model resolution was varied in tandem with the horizontal friction and in the bottom row the bottom friction was increased 10-fold to damp the eddy-driven abyssal circulation. East of 68ºW all of the simulations give similar, generally-realistic Gulf Stream pathways, except near 50ºW, where the simulations with a DWBC exhibit two mean pathways (inner and outer meanders) at the location of the Gulf Stream transition to the North Atlantic Current as it rounds the southern tip of the Grand Banks, a phenomenon discussed dynamically in Hurlburt and Hogan (2008). All three of the simulations with a DWBC and one of the simulations without it exhibit a realistic mean Gulf Stream pathway west of 68ºW, but the other two simulations without a DWBC

exhibit pathways that overshoot the observed separation latitude in accord with the constraint of linear theory on the flow. These results indicate an abyssal current impact on the pathway west of 68ºW.

To investigate the impacts of abyssal currents on the Gulf Stream pathway, we use a two-layer theory for abyssal current steering of upper ocean current pathways (Hurlburt and Thompson, 1980; Hurlburt et al., 1996, 2008b). In a two-layer model with no diapycnal mixing, the continuity equation for layer 1 is

$$h_{1t} + \mathbf{v}_1 \cdot \nabla h_1 + h_1 \nabla \cdot \mathbf{v}_1 = 0 \qquad (1)$$

where h_1 is upper layer thickness, $_t$ is the time derivative and $\mathbf{v_i}$ is the velocity in layer i. The geostrophic component of the advective term in (1) can be related to the geostrophic velocity ($\mathbf{v_{ig}}$) in layer 2 by

$$\mathbf{v_{1g}} \cdot \nabla h_1 = \mathbf{v_{2g}} \cdot \nabla h_1 \qquad (2)$$

because from geostrophy,

$$\mathbf{k} \times f (\mathbf{v_{1g}} - \mathbf{v_{2g}}) = -g' \nabla h_1, \qquad (3)$$

$\mathbf{v_{1g}} - \mathbf{v_{2g}}$ is parallel to contours of h_1. In (3) $\mathbf{k}$ is a unit vector, $f = 2\omega\sin\theta$ is the Coriolis parameter, ω is the Earth's rotation rate ($7.292 \times 10^{-5} s^{-1}$), θ is latitude, $g' = g(\rho_2-\rho_1)/\rho_2$ is the reduced gravity due to buoyancy, $g = 9.8$ m s^{-2} is the gravitational acceleration of the Earth, and ρ_i is the water density in layer i. Since geostrophy is typically a very good approximation outside the equatorial wave guide and normally near-surface currents are much stronger than abyssal currents, then usually $|\mathbf{v_1}| \gg |\mathbf{v_2}|$, making ∇h_1 a good measure of $\mathbf{v}_1$ under these conditions. From the preceding we see that abyssal currents can advect upper layer thickness gradients and therefore the *pathways* of upper ocean currents. Abyssal current advection of upper ocean current pathways is strengthened when strong abyssal currents intersect upper ocean currents at nearly right angles, but often the end result of this advection is near barotropy because the advection is reduced as $\mathbf{v_1}$ and $\mathbf{v_2}$ become more nearly parallel (or antiparallel).

This theory has proven useful in understanding the dynamics of ocean models with higher vertical resolution, when all of the following conditions are satisfied: (a) the flow is nearly geostropically balanced, (b) the barotropic and first baroclinic modes are dominant, and (c) the topography does not intrude significantly into the stratified ocean. Additionally, the interpretation in terms of near-surface currents applies when $|\mathbf{v_{near\ sfc}}| \gg |\mathbf{v_{abyssal}}|$. Note the theory does not apply at low latitudes because of (a) and (b), but should be useful in large parts of the stratified ocean, even where current systems are relatively weak, as seen in the well-stratified southern half of the Japan/East Sea (Hurlburt et al., 2008b). While abyssal currents driven by any means can steer upper ocean current pathways, baroclinic or mixed barotropic-baroclinic

instability is an important source of abyssal currents because baroclinic instability is very effective in transferring energy from the upper to abyssal ocean. These eddy-driven abyssal currents are constrained to follow the geostrophic contours of the topography and in turn can steer the pathways of upper ocean currents, including their mean pathways. This upper ocean - topographic coupling via flow instabilities requires that the physics of baroclinic instability be very well resolved in order to obtain sufficient downward transfer of energy. As a result, this type of coupling is a key criterion in distinguishing between eddy-resolving and eddy-permitting ocean simulations, in regions where it occurs, along with the first baroclinic Rossby radius of deformation and realistic eastward penetration of inertial jets, as discussed in Hurlburt et al. (2008b). This coupling also highlights the need for eddy-resolving ocean models in ocean prediction systems and in climate prediction models, as discussed in Hurlburt et al. (2008a, 2009).

Based on the preceding discussion, we look in Figure 3 for abyssal currents west of ~68ºW that may advect the simulated Gulf Stream pathways in Figure 2. We start with the simulation shown in Figures 2c and 3c because it has 1/32º resolution, the standard bottom friction, and a DWBC. In that simulation abyssal currents pass under the Gulf Stream near 68.5ºW, 72ºW, and the western boundary, all generally southward. The abyssal currents near 68.5ºW and 72ºW cross under at large angles and could clearly advect the Gulf Stream pathway, but the abyssal current adjacent to the western boundary is nearly antiparallel as it crosses under the Gulf Stream, a point noted by Pickart (1994) based on observations, and thus has a weak steering effect on the Gulf Stream pathway. The corresponding simulation without a DWBC (Figures 2d and 3d) has nearly the same Gulf Stream pathway with an even stronger abyssal current crossing under it near 68.5ºW. The two other simulations without a DWBC have only a weak mean abyssal current crossing under it at this longitude (<3 cm sec^{-1}), while all of the simulations with realistic Gulf Stream separation have a more robust abyssal current passing under the Gulf Stream near 68.5ºW (>4 cm sec^{-1}). None of the simulations without a DWBC have an abyssal current crossing under near 72ºW, while all of the simulations with a DWBC have one fed by two branches from the north side. The 1/32º simulations with a DWBC and standard (Figures 2c and 3c) or high bottom friction (Figures 2e and 3e) have nearly the same Gulf Stream pathway between the western boundary and 68ºW, but in the simulation with high bottom friction the abyssal currents crossing under the Gulf Stream near 72ºW are extremely weak. Thus, the abyssal current crossing under the Gulf Stream near 68.5ºW is clearly the one that is essential for the model's simulation of a realistic Gulf Stream pathway between the western boundary and 68ºW. Further, the DWBC is not necessary for simulation of a realistic Gulf Stream pathway, but it augments the key abyssal current sufficiently for that to occur in the two simulations with the weaker eddy-driven abyssal circulations.

The 1/32º simulation with standard bottom friction and a DWBC (Figure 3c) is used in a zoom of the mean abyssal currents with the addition of topographic contours (Figure 4a). The

plotted contours are for the vertically-uncompressed (real) topography to facilitate comparisons between model and observed abyssal currents in relation to topographic features. Figure 4b depicts mean abyssal currents and uncompressed topography from a corresponding 1/8º eddy-permitting simulation over a larger region with the zoom region in Figure 4a marked with a box. Unlike the 1/32º simulation (Figure 4a), the abyssal circulation in the 1/8º model is dominated by the DWBC and the eddy-driven abyssal circulation is extremely weak (Figure 4b). In particular, the 1/8º model does not simulate the key abyssal current near 68.5ºW. The DWBC augments this current in two of the simulations (Figures 3a and 3e) because the DWBC and the eddy-driven abyssal circulation interact and become intertwined in the eddy-resolving simulations. The surface circulation in the 1/8º model is basically a wiggly version of the linear solution (shown in Hurlburt and Hogan, 2000), who also present numerous model-data comparisons for the 1/16º simulation in Figures 2a and 3a and the 1/32º simulation in Figures 2c and 3c.

In addition to the abyssal current adjacent to the western boundary, abyssal currents are seen crossing under the Gulf Stream via three different pathways centered over different isobaths between the western boundary and 68ºW. North of the Gulf Stream these pathways are centered over the 4200 m, 3700 m, and 3100 m isobaths, the first crossing under near 68.5ºW, the other two crossing under in a confluence near 72ºW. All three abyssal currents cross isobaths to deeper depths while passing under the Gulf Stream. They do this to conserve potential vorticity in relation to the downward north to south slope of the base of the thermocline in accord with the theory of Hogg and Stommel (1985). The two currents over deeper isobaths retroflect into the interior, taking a variety of simple to complex pathways (complex even in the mean, e.g. Figure 3c) before all emerge in a single strong abyssal current along a gentle escarpment. That current exits Figure 4a near 72ºW and rejoins the DWBC near 32ºN. In contrast, the branch centered over the 3100 m isobath north of the stream continues along the continental slope south of the stream (centered above the 3700 m isobath). Each cross-under pathway is influenced by specific features of the topography and each also flows along one side of an associated eddy-driven abyssal gyre centered directly beneath the Gulf Stream. These gyres are located in regions where the slopes of the topography and the base of the thermocline are matched closely enough to create regions of quite uniform potential vorticity for abyssal currents, as shown in Hurlburt and Hogan (2008). The shallowest and westernmost gyre is anticyclonic, while the two associated with eastward retroflections into the interior are cyclonic, all three in accord with the sign of the relative vorticity generated due to topographic constraints on the pathways of the associated abyssal currents as they cross under the Gulf Stream (shown in Hurlburt and Hogan, 2008).

2.3 Observational evidence of abyssal currents in the Gulf Stream region

Figure 5b (from Johns et al., 1995) presents observational evidence for the key abyssal current crossing under the Gulf Stream near 68.5ºW, including current speeds similar to the model, currents crossing isobaths to deeper depths beneath the Gulf Stream, and a closed cyclonic circulation. Additionally, the currents along the shallowest isobaths within the

observational array flow along isobaths that would feed into the retroflecting abyssal current that crosses under the Gulf Stream near 72ºW. Figure 6 (from Pickart and Watts, 1990) provides a composite of historical measurements of abyssal currents 100 to 300 m above the bottom. It provides striking evidence of the complete cyclonic abyssal gyre centered near 37ºN, 71ºW with current speeds similar to the model. Another salient observation is the ~12.5 cm sec^{-1} west-southwestward current near 34.5ºN, 71.1ºW that corroborates the strong abyssal current along the gentle escarpment in Figure 4a (10.5 cm sec^{-1} at the same location in the model).

Like the model (Figure 4a), the observation-based abyssal current schematic of Schmitz and McCartney (1993, their Figure 12a) depicts a retroflecting abyssal current pathway that later rejoins the DWBC, in addition to a pathway that continues along the continental slope. These two pathways are also consistent with Range and Fixing of Sound (RAFOS) float trajectories at 3500 m depth discussed in Bower and Hunt (2000). RAFOS floats that crossed under the Gulf Stream west of ~71ºW continued generally southward along a deeper isobath of the continental slope, while floats crossing under east of ~71ºW retroflected into the interior, most of them taking complex eddying trajectories, but of the six retroflecting trajectories shown, the one that crossed under at the location of the key abyssal current (near 69ºW) (their Figure 7j) took an eddying trajectory en route to a small amplitude double retroflection, first to the east (at 36.7ºN, 70.1ºW) and then to the west (at 36.0ºN, 68.4ºW) before rapidly following a nearly straight-line trajectory along the gentle escarpment, an overall trajectory in good agreement with the model mean in Figure 4a and one that provides additional evidence for the strong eddy-driven abyssal current along the gentle escarpment (seen in the southern part of Figure 4a). This abyssal current is completely absent in the 1/8º eddy-permitting simulation (Figure 4b).

2.4 Gulf Stream separation and pathway dynamics, Part I: Abyssal current impact

An eddy-driven abyssal current, bottom topography, and a Gulf Stream feedback mechanism constrain the latitude of the Gulf Stream near 68.5ºW. To help illustrate the steps explaining this statement, Figure 7 depicts the mean depth of the base of the model thermocline overlaid with the same mean abyssal currents and topographic contours as Figure 4a. The results are from the same 1/32º simulation with a DWBC shown in Figures 2c, 3c, and 4a.

The steps in the explanation are (1) an eddy-driven abyssal current, possibly augmented by the DWBC, approaches from the northeast and advects the Gulf Stream pathway southward, i.e. prevents the overshoot pathway seen in Figures 2b and 2f. (2) To conserve potential vorticity, the abyssal current crosses to deeper depths while passing under the Gulf Stream (Hogg and Stommel, 1985), a feedback mechanism that allows the Gulf Stream to help determine its own latitude. (3) Due to the topographic configuration, the passage to deeper depths requires curvature toward the east and generation of positive relative vorticity. (4) Once the abyssal current becomes parallel to the Gulf Stream, further southward advection of the Gulf Stream pathway is halted. (5) The local latitude of the Gulf Stream is determined by the northernmost

latitude where the abyssal current can become parallel to the Gulf Stream. (6) Due to constraints of the local topographic configuration on this process, the resulting local Gulf Stream latitude is not very sensitive to the strength of the abyssal current, once it is sufficient to perform the advective role. However, the results of these dynamics would be sensitive to the location of abyssal currents in relation to the isobaths, the accuracy of the model in representing key topographic features, and the depth change in the base of the thermocline across the Gulf Stream.

Essentially the same explanation can be applied to the effects of the abyssal current crossing under the Gulf Stream near 72ºW and to abyssal currents that develop either cyclonic or anticyclonic curvature and become either parallel or antiparallel to the Gulf Stream while crossing underneath. However, the response to the abyssal current near 72ºW is minimal as evidenced in Figures 2 and 3 and an impact is visible only in the 1/32º simulation with a DWBC and standard bottom friction ($C_b = .002$) (Figure 2c). In Figure 2c there is a straightening of the Gulf Stream pathway over ~73-70ºW not seen in the other figure panels. This phenomenon is also evident in the overlaid mean Gulf Stream IR northwall frontal pathway and in the Gulf Stream pathway as depicted by the 12ºC isotherm at 400 m depth, the latter shown in Watts et al. (1995). The reason for the slight impact of this abyssal current on this Gulf Stream simulation is discussed in the next subsection.

Additionally, it should be noted that the scale of the eddy-driven mean abyssal gyres beneath the Gulf Stream is similar to the width of the stream (Figure 5) and related to regions of nearly uniform potential vorticity beneath the stream (Hurlburt and Hogan, 2008) where slopes of topography and the base of the thermocline are quite well matched. These gyres are not related to mean meanders in the Gulf Stream. In contrast, the Kuroshio exhibits two mean northward meanders just east of where the Kuroshio separates from the coast of Japan, meanders that are dynamically related to eddy-driven mean abyssal gyres, as discussed in Hurlburt et al. (1996, 2008b).

2.5 Gulf Stream boundary separation as an inertial jet following a constant absolute vorticity (CAV) trajectory

Constraint of the Gulf Stream latitude near 68.5ºW is not a sufficient explanation of the Gulf Stream pathway between the western boundary and 69ºW. Further, the abyssal current crossing under the Gulf Stream near 72ºW demonstrated little effect on the pathway. Thus, there must be another essential contribution to Gulf Stream pathway dynamics over that longitude range. Using along-track data from four satellite altimeters, Figure 8 depicts only a narrow band of high SSH variability along the Gulf Stream west of 69ºW, indicating a relatively stable pathway segment in that region. Thus, we test the relevance of a particular type of theoretical inertial jet pathway, namely a CAV trajectory (Rossby, 1940; Haltiner and Martin, 1957; Reid, 1972; Hurlburt and Thompson, 1980, 1982). In a nonlinear 1.5 layer reduced-gravity model, a CAV trajectory requires a frictionless steady free jet with the streamline at the core of the current

following contours of constant SSH and layer thickness. The latter requires geostrophic balance so that conservation of potential vorticity becomes conservation of absolute vorticity along a streamline at the core of the current. Accordingly, the simulations in Figure 2 were tested to see if (a) the mean path of the current core in the top layer of the model (black line in Figure 9) overlaid an SSH contour (yellow-green line in Figure 9) and (b) there was a narrow band of high SSH variability along the current core between the western boundary and 69ºW (plotted in color in Figure 9).

Following Reid (1972) and Hurlburt and Thompson (1980, 1982), the CAV trajectories were calculated from

$$\cos\alpha = \cos\alpha_o + \tfrac{1}{2}y^2/r^2 - y/\gamma_o , \qquad (4)$$

which is an integrated form of the differential equation that assumes the velocity at the core of the current, υ_c, is a constant and where $r = (\upsilon_c/\beta)^{1/2}$, β is the variation of the Coriolis parameter with latitude, α is the angle of the current with respect to the positive x-axis on a β-plane, y is the distance of the trajectory from the x-axis, γ is the trajectory radius of curvature, and the subscript $_o$ indicates values at the origin of the trajectory calculation (here at an inflection point where $\gamma_o \rightarrow \infty$). The amplitude (b) (here the northernmost point) of the trajectory in relation to the inflection points can be calculated from

$$b = 2r \sin\tfrac{1}{2}\alpha_o . \qquad (5)$$

In order for the Gulf Stream to separate from the western boundary as a free jet following a CAV trajectory, the CAV trajectory must be initialized with a trajectory inflection ($\gamma_o \rightarrow \infty$) located at the separation point. Since the angle of separation (α_o) is north of due east, the CAV trajectory must subsequently develop curvature that is concave toward the south. If the simulation exhibits curvature to the north after separation, then it does not separate from the western boundary as a free jet, even through it may have one or more segments downstream that follow a CAV trajectory.

The calculated CAV trajectories are overlaid as red curves on Figure 9. Details of the CAV trajectory calculations can be found in Table 2 of Hurlburt and Hogan (2008). The speed at the core of the current (υ_c) near separation from the western boundary is 1.6 - 1.7 m sec^{-1} in the 1/16º simulations and 1.9 - 2.0 m sec^{-1} in the 1/32º simulations, in line with observations of 1.6 - 2.1 m sec^{-1} reported in Halkin and Rossby (1985), Joyce et al. (1986), Johns et al. (1995), Schmitz (1996), and Rossby et al. (2005). A model mean υ_c over 75 - 70ºW was used in the CAV trajectory calculations. The angle of separation is 53±3º north of due east for the simulations with a realistic pathway and the inflection points used to initialize the CAV trajectory calculations are marked by red dots on the trajectories.

The four simulations with a realistic Gulf Stream pathway demonstrate close agreement between the model pathway, as represented by υ_c, and the corresponding CAV trajectory. However, the two simulations with pathways that overshoot the latitude of the observed Gulf Stream pathway exhibit curvature to the north immediately after separation and an inflection point (red dot) located northeast of separation from the western boundary. That means they do not separate from the western boundary as a free jet, but instead indicate a strong influence from the constraints of linear dynamics (Figure 1). Thus, CAV trajectory dynamics alone are not sufficient to explain the Gulf Stream pathway between the western boundary and 69ºW. However, they do explain the small impact of the abyssal current crossing under the Gulf Stream near 72ºW (Figure 5), because the abyssal current and the CAV trajectory give nearly the same Gulf Stream latitude at that location (Figure 9c).

2.6 Gulf Stream separation and pathway dynamics, Part II: Role of CAV trajectories

In the simulations with a realistic Gulf Stream, the mean pathway closely follows a CAV trajectory between its separation from the western boundary and ~70ºW. The CAV trajectory depends on (1) the angle of boundary current separation (with respect to latitude), as largely determined by the angle of the shelf break prior to separation, (2) the speed at the core of the current, and (3) an inflection point located where boundary current separation occurs.

2.7 Gulf Stream separation and pathway dynamics, Part III: The cooperative interaction of abyssal currents and CAV trajectories

Neither abyssal currents nor CAV trajectories alone are sufficient to explain Gulf Stream separation from the western boundary and its pathway to the east. Abyssal current constraint of the Gulf Stream latitude near 68.5ºW, in conjunction with the topographic configuration and a Gulf Stream feedback mechanism, is not a sufficient explanation of the Gulf Stream pathway between the western boundary and 68ºW. Gulf Stream simulations with realistic speeds at the core of the current are not sufficiently inertial (a) to overcome the linear solution demand for an overshoot pathway and (b) to obtain realistic separation without assistance from the abyssal current near 68.5ºW. Thus a CAV trajectory and the constraint on the latitude of the Gulf Stream near 68.5ºW work together in simulation of a realistic Gulf Stream pathway between the western boundary and 68ºW.

The eddy-driven abyssal circulation is sufficient to obtain the key abyssal current, which was not simulated without it. The DWBC is not necessary, but did augment the key abyssal current and did assist the eddy-driven abyssal circulation in effecting realistic Gulf Stream separation, when the latter was not strong enough by itself. The impact of the DWBC on Gulf Stream separation was resolution dependent, required at 1/16º, but not at 1/32º resolution.

Finally, the dynamical explanation is robust. As long as the speed at the core of the current was consistent with observations and the key abyssal current was sufficiently strong, the

simulated Gulf Stream separation and its pathway to the east were in close agreement with observations despite differences in model resolution, bottom friction, strength of the abyssal circulation, and the presence or absence of a DWBC. Further, the explanation is consistent with a wide range of key observational evidence in the upper and abyssal ocean, including a 15-year mean Gulf Stream IR northwall pathway, the speed at the core of the current near Gulf Stream separation, the pattern of sea surface height variability from satellite altimetry, and mean abyssal currents. Hurlburt and Hogan (2000) present a large number of additional model-data comparisons for the simulations depicted in Figures 2a and 2c.

3. Dynamical evaluation of Gulf Stream simulations by eddy-resolving global and basin-scale OGCMs

Significant success has been achieved in simulating the Gulf Stream pathway in eddy-resolving basin-scale OGCMs with high vertical resolution, but at the same time simulations have been very sensitive to changes, such as subgrid scale parameterizations and parameter values. Thus, it has been difficult to obtain consistent results and many simulations have exhibited serious flaws (Paiva et al., 1999; Smith et al., 2000; Bryan et al., 2007; Chassignet and Marshall, 2008; Hecht and Smith, 2008; Hecht et al., 2008). In this section we perform a dynamical evaluation of eddy-resolving global and basin-scale OGCM simulations of Gulf Stream separation and its pathway to the east. The immediate goals are to better identify and understand the sources of success and failure, and the impacts of data assimilation. Future goals are improved and more consistently realistic simulations of the Gulf Stream, increased ability to nowcast and forecast it on time scales up to a month, improved climate prediction in the Gulf Stream region, and increased efforts to dynamically evaluate OGCMs in other regions.

A set of eddy-resolving global and basin-scale simulations from HYCOM, MICOM, NEMO, and POP are used in the evaluation. In addition to simulations with a realistic Gulf Stream pathway and dynamics consistent with observations, simulations with several types of flaws are evaluated, including (a) overshoot pathways, (b) a realistic pathway with unrealistic dynamics, (c) premature separation south of Cape Hatteras (the observed location), (d) pathways that separate at Cape Hatteras but have a pathway segment that is too far south east of the separation point, (e) dual pathways after separation, and (f) pathways impacted by unrealistic behavior upstream of the separation point, such as excessive variability or large loops away from the observed mean pathway along the shelf break.

To streamline the evaluation for the purpose of this discussion, we focus on the following: (1) To evaluate the mean path, mean SSH from the model is overlaid by the 15-year mean Gulf Stream IR northwall pathway ± 1 standard deviation by Cornillon and Sirkes (unpublished). This frontal pathway has 0.1º longitudinal resolution and lies along the northern edge of the Gulf

Stream. (2) SSH variability and abyssal eddy kinetic energy (EKE) are used to help identify the dynamics of Gulf Stream pathway segments and source regions for eddy-driven mean abyssal currents. (3) Mean speed at the core of the current is used to assess whether or not the simulated Gulf Stream inertial jet is consistent with observations near the western boundary. (4) The DWBC and eddy-driven mean abyssal currents can influence simulated mean Gulf Stream pathways and, depending on their strength and location in relation to the isobaths, have the potential to improve or increase the errors in the simulated pathways. (5) Both the strength and depth structure of the AMOC can affect the Gulf Stream pathway. Increasing the strength can make the simulated Gulf Stream more inertial, but can also increase the tendency for an overshoot pathway based on linear dynamics. The depth structure of the AMOC influences the depths of the isobaths followed by the DWBC and interactions between the DWBC and the eddy-driven abyssal circulation. (6) The basin-wide linear solution response to the mean wind stress forcing yields the constraints of linear dynamics on the strength and pathways of wind-driven currents in the Gulf Stream region.

In the dynamical evaluation we focus on a segment of the Gulf Stream that extends from 30ºN, 80ºW, upstream of the observed separation latitude near 35ºN, 75ºW, to about 68ºW, and characterizations of accuracy refer to pathway segments and other features within that region, even though a larger region may be depicted in some figures. First we focus on three simulations without data assimilation, one from 1/12º Atlantic MICOM with a realistic Gulf Stream pathway and two with commonly-simulated erroneous pathways, namely a pathway that overshoots the observed separation latitude (from 1/12º Atlantic HYCOM) and one that exhibits premature separation and a subsequent pathway segment that lies south of the observed latitude (from 1/12º Atlantic NEMO). It should be noted that all three models have provided simulations with a realistic Gulf Stream pathway as well as a variety of unrealistic pathways, a topic of discussion in the lecture. Additionally, 1/16º resolution in Section 2 is approximately equal to 1/12º resolution in Sections 3 & 4 (~7 km at mid-latitudes) because simulations in Section 2 are characterized by mid-latitude resolution (in º) and in Sections 3 & 4 by equatorial resolution.

3.1 Simulation with a realistic Gulf Stream pathway

Figure 10 presents the mean SSH and SSH variability from the three simulations. In the MICOM simulation the mean IR northwall frontal pathway (in red) closely follows the northern edge of the simulated Gulf Stream and there is an associated narrow band of high SSH variability west of 69ºW. The mean core speed of the current near the separation point is 1.55 m sec^{-1}, at the low end of the observational evidence.

In representing the mean abyssal currents, a depth average from ~3000 m to the bottom is appropriate, but layer 15 in MICOM is very thick. Since MICOM is isopycnal, the layer interfaces vary in depth, but typically the top of layer 15 is ~2000 m and the bottom is ~3600 m. Although depths this shallow in some OGCM simulations include features that are not bottom

trapped (e.g. see Figure 8 and related discussion in Hecht and Smith, 2008), such features are not evident when layer 15 is included in the MICOM depth average over the abyssal layers (Figure 11a). The current segments that cross under the Gulf Stream to deeper depths near 72ºW and 68.5ºW are weaker by ~1 cm sec^{-1} (one color contour) when layer 15 is included, but that is the most negative effect. Otherwise, adding layer 15 gives a broader picture of the MICOM abyssal circulation.

The mean abyssal circulation in MICOM (Figure 11) depicts the key abyssal current observed crossing under the Gulf Stream near 68.5ºW (Figure 5), the observed cyclonic gyre centered near 37ºN, 71ºW, and the strong current observed along the gentle escarpment at 34.5ºN, 71.1ºW (Figure 6). It is also consistent with the RAFOS float trajectory in Bower and Hunt (2000, their Figure 7j) and the observation-based schematic in Schmitz and McCartney (1993, their Figure 12a), both described in Section 2.3. These features in MICOM are very similar to those in Figure 4a, including similar dual pathways approaching the Gulf Stream cross-under near 72ºW. In both cases the eastern pathway crosses under and retroflects to the east, while the western one continues along the continental slope, the latter via different pathways in MICOM and Figure 4a. In MICOM the western pathway follows a sharp westward turn in the 3200 m isobath along the northern edge of the simulated Gulf Stream, while in Figure 4a it crosses under the Gulf Stream and continues along the 3600-4000 m isobaths of the continental slope south of the stream. RAFOS float trajectories at ~3500 m depth in Bower and Hunt (2000, their Figure 7) support the existence of this deeper pathway along the continental slope, which is missing in the MICOM simulation.

At >30 Sv in the latitude range of Figure 10, the AMOC in MICOM (Figure 12a) is the strongest of all the simulations considered here, but at the same time the mean speed of the current core near separation is relatively weak, suggesting a relatively weak wind-driven contribution and a strong contribution to the abyssal circulation from the AMOC. The depth range of the incoming DWBC (Figure 11a) is conducive to the realistic abyssal current pathways simulated by MICOM.

3.2 Simulation with a pathway that overshoots the observed latitude

Overshooting pathways are more characteristic of eddy-permitting simulations (Bryan et al., 2007), but they can also occur in eddy-resolving simulations, e.g., the 1/12º Atlantic HYCOM simulation shown in Figure 10b. The mean over years 3-6 of the simulation yielded a realistic Gulf Stream pathway (not shown), but over time the simulation developed the overshoot pathway shown in the mean over years 11-13 in Figure 10b. Due to a change in the sea surface salinity relaxation, the salinity in the Gulf Stream and in pathways all the way to the Nordic Seas increased over time. As a result, the salinity and density of the Denmark Straits overflow into the subpolar Atlantic also increased. In addition, the strength of the AMOC increased from a mean of ~22 Sv over years 3-6 (not shown) to ~30 Sv over years 11-13 in the latitude range of

interest (Figure 12b). In the process the mean core speed of the Gulf Stream near separation increased from 1.7 to 2.1 m sec^{-1}, making it the most inertial at separation of all the simulations considered and at the top end of observational values. We know from Section 2 that the AMOC contributes to the demands of linear dynamics for an overshoot pathway, but why did that happen in this simulation and not in the MICOM simulation, which has a slightly stronger AMOC and a less inertial Gulf Stream near separation?

The AMOC of the HYCOM simulation is relatively concentrated over 2000-3000 m depth in the latitude range of Figure 11, while the AMOC from MICOM is more uniformly distributed with depth. Correspondingly, the DWBC in the HYCOM simulation is concentrated along shallower isobaths than in the MICOM simulation. To facilitate discernment of the relationships between near-surface currents, abyssal currents, and the topography, mean currents at the depth of the current core are overlaid with topographic contours in the same region as the abyssal currents (Figure 13).

In Figure 13 the simulated Gulf Stream follows the shelf break and continental slope to a location east of 72ºW, where a ridge in the topography exists in the depth range 2200-2800 m. There the main core of the current separates from the continental slope and the inshore portion continues along the shelf break and continental slope. The source of this bifurcation is a strong southward abyssal current nearly perpendicular to the Gulf Stream along the eastern side of the ridge. Most of that current then becomes antiparallel to the Gulf Stream along the south side of the ridge. Since there is no ridge inshore of ~2200 m, the inshore portion of the bifurcation continues along the shelf break. An additional portion on the inshore side of the stream joins the portion along the shelf break between 69 and 67ºW, where the joining current flows nearly parallel to the isobaths and antiparallel to the underlying strong abyssal currents.

At the location where the main core of the simulated Gulf Stream separates from the continental slope, the underlying abyssal current also bifurcates. The main branch continues westward along the continental slope until most of it crosses southward under the Gulf Stream along the western slope of a valley west of 72ºW, while the second branch continues southward under the Gulf Stream east of 72ºW, again along the western slope of a valley. In the process both abyssal currents cross isobaths from 2600 to 3400 m depth beneath the Gulf Stream, in accord with the theory of Hogg and Stommel (1985), before joining a southwestward abyssal current along the 3200-3600 m isobaths that flows nearly antiparallel along the southeastern side of the simulated Gulf Stream.

East of 71ºW there is evidence that abyssal currents play a role in splitting the main jet, with the northern branch continuing eastward along 38-39ºN and the southern branch forming a large meander. South of ~38ºN and the 3900 m isobath, there is a broad southward abyssal flow (straddling 70ºW) that advects the southern branch southward and crosses isobaths to ~4500 m. A second abyssal current, generally centered along the 4800 m isobath, crosses southward under

the northern branch between 65 and 66ºW and then turns nearly westward with the isobath and becomes antiparallel to the northern branch until it reaches the center of the meander trough, where it joins the first one. The meander lies in a region of high SSH variability (Figure 10e) and high abyssal EKE (not shown), evidence that the mean abyssal gyre, centered near 37ºN, 68ºW is eddy-driven via baroclinic instability.

3.3 Simulation with premature separation from the western boundary

The 1/12º Atlantic NEMO simulation exhibits premature separation from the western boundary near 34ºN. Like the HYCOM simulation the Gulf Stream core speed near separation is toward the high end of the observational evidence (1.9 m sec^{-1}). However, at 20 Sv in the latitude range of Figure 10, the AMOC is much weaker than in the MICOM and HYCOM simulations (but still slightly high), indicating a stronger wind-driven contribution to the simulated Gulf Stream than in the other two simulations. In addition, the southward transport of the AMOC lies between ~1000 and 3500 m within the latitude range of Figure 10, a depth structure largely set by the southern boundary. Also, within the latitude range of Figure 10 a relatively large amount of deep water formation occurs compared to the other two simulations (Figure 12).

In Figure 11c the relationship between the mean abyssal circulation (below 2800 m) and the simulated Gulf Stream pathway is obvious, a mean abyssal current crossing under the Gulf Stream where it separates from the western boundary. In the process the abyssal flow crosses the 3300-4400 m isobaths. The cross-under is fed by an abyssal current along the ~3200-3600 m isobaths as well as abyssal currents along continental slope isobaths shallower than 2800 m. A similar abyssal current along the 3200-3600 m isobaths is seen in the HYCOM simulation (Figure 11b), but in that case the current lay east of the overshooting Gulf Stream pathway. The NEMO simulation is missing abyssal currents along the 3100 and 4100-4400 m isobaths that crossed under the Gulf Stream in the MICOM simulation, the latter near 68.5ºW as a consequence of the shallow AMOC. The simulated Gulf Stream pathway generally parallels the underlying abyssal current to the east. A secondary eastward current splits from the north side of the main current between 71 and 70ºW, following a pathway antiparallel to underlying abyssal currents, but south of the strongest ones. This split-off is unrelated to abyssal currents, suggesting the possibility of a linear wind-driven response, as the main pathway became less inertial.

3.4 Discussion

In the three simulations, high sensitivity to the strength and vertical structure of the AMOC is evident at 1/12º resolution. The sensitivity to the depth structure of the AMOC is evident via the abyssal currents and their relationship to the isobaths. As in Section 2, even Gulf Stream core speeds at the top end of the observational evidence near separation were not sufficient to

effect a realistic Gulf Stream pathway between the western boundary and 68ºW without assistance from abyssal current steering of the simulated pathway. The results in Section 2 suggest that doubling the resolution would reduce simulation sensitivity to the AMOC by increasing the inertial character of the simulated Gulf Stream and increasing the strength of the eddy-driven abyssal circulation. In the lecture, results from a 1/25º global HYCOM simulation will be included and compared to those from a corresponding 1/12º global simulation.

4. Impact of data assimilation on model dynamics in the Gulf Stream region

To investigate the impact of data assimilation on the Gulf Stream pathway we use a set of four 1/12° global HYCOM experiments, two non-assimilative, one with climatological atmospheric forcing and the second forced interannually, and two data-assimilative hindcasts, each using a different method for downward projection of SSH. The base simulation for these experiments was forced by an ECMWF climatology for the surface momentum and heat fluxes. The mean Gulf Stream is given by the last four years of the spin-up (years 12-15), which is designated as "climatological". The second simulation for the experiment is initialized from the end of the climatologically forced simulation and is forced interannually over the period 2003 to 2007. It uses the Navy Operational Global Atmospheric Prediction System (NOGAPS) fluxes with an adjustment of the temporal mean winds to the ECMWF climatology and with a scaling of the 10 m wind speed anomalies based upon QuikScat wind speed statistics (Kara et al., 2009). For this discussion, the mean is taken over the last 3 years, which is designated as "interannual". In both of the hindcasts, the data are assimilated into 1/12° global HYCOM via the Navy Coupled Ocean Data Assimilation system (NCODA, Cummings, 2005) using a multivariate optimal interpolation. The difference between the two hindcasts is the treatment of the altimetric sea surface height anomalies (SSHA). The first hindcast, designated as "C-H assimilation", is a twin of the non-assimilative interannually forced simulation with the SSHA extended into the ocean interior via the technique of Cooper and Haines (1996) and with the climatologically-forced model mean sea surface in the Gulf Stream region adjusted to the observed mean pathway using a rubber-sheeting technique (Smedstad et al., 2003). The second hindcast, designated as "MODAS assimilation", uses the Modular Ocean Assimilation System (MODAS, Fox et al., 2002, Barron et al., 2007) to extend the SSHA into the ocean interior via synthetic profiles of temperature and salinity.

4.1 Climatologically forced simulation with a realistic pathway

The mean velocity in layer 6, approximately 25 m in depth, from each of the four experiments is shown in Figure 14 along with the 15-year mean IR northwall pathway. For the climatologically forced simulation, the Gulf Stream tracks the mean IR pathway west of 68°W and tends north of the IR pathway east of 68°W. The Eulerian mean core speed near the

separation point is 1.3 m sec^{-1}. It decreases rapidly to the east with a speed of 0.8 m sec^{-1} near 72°W and < 0.25 m sec^{-1} near 68°W. The weak Gulf Stream is associated with weak mean abyssal currents, as shown in Figure 15a. The key southward abyssal current at 72°W is weak, with a mean speed < 4 cm sec^{-1}, and the key current at 68.5°W is absent as are the associated deep cyclonic gyres seen in observations (Figures 5 and 6). The AMOC also is weak and shallow with a transport < 13 Sv (Figure 16a). (1) The large area of high SSH variability west of 68°W (Figure 17a), (2) the well-defined southern recirculation gyre west of 70°W (Figure 14a), (3) the eddy-driven mean abyssal gyre centered directly beneath the surface gyre over relatively flat topography (Figure 15a), and (4) the associated high deep EKE (not shown) are evidence of strong baroclinic instability in the region. The separating Gulf Stream pathway lies along the northern edge of the associated recirculation gyres. The location of the eddy-driven mean abyssal gyre relative to the southern edge of the separating jet and the location of the northwestern most flat topography suggests a topographic role in the separating pathway driven by baroclinic instability of the separating jet, because baroclinic instability and the eddy-driven abyssal gyre would be inhibited if positioned farther north over the sloping topography. Thus, while the resulting 4-year mean pathway is quite realistic, the dynamics of the separating jet are unrealistic, the mean core speed near separation is below the range of observational evidence, the AMOC is too shallow and too weak, and the simulation is inconsistent with the observed SSH variability and relevant abyssal current observations.

4.2 Interannually forced simulation with premature separation

The climatologically forced simulation serves as the initial condition for the interannually forced simulation. The 3 year mean Gulf Stream separates from the coast prematurely between 34°N and 35°N, similar to the 1/12° Atlantic NEMO simulation. The mean core speed in layer 6 (~25 m) near the separation point is 1.6 m sec^{-1}, but the speed decreases rapidly to the east with Eulerian mean core speeds of only 0.9 m sec^{-1} at 75°W and < 0.5 m sec^{-1} at 72°W (Figure 14b). The Gulf Stream splits near 70°W with part of the flow retroflecting in a strong recirculation gyre and remainder flowing northeastward similar to a linear wind-driven/AMOC response as the Gulf Stream becomes weaker and less inertial. The abyssal flow shown in Figure 15b is very weak north of about 36°N. The key abyssal currents at 72°W and 68.5°W and the associated cyclonic gyres are absent. The eddy-driven abyssal circulation, with speeds < 8 cm sec^{-1}, flows under the Gulf Stream near 35°N, 72°W helping to steer the flow southward into the recirculation gyre. The AMOC is very shallow and weak, with transport < 13 Sv (Figure 16b). The SSH variability in Figure 17b shows evidence of premature separation, a strong recirculation gyre and eddies shed from the northern branch near 70°W, north of the separating jet.

4.3 Cooper-Haines data assimilation

The data assimilative interannual simulation starts from end of the climatological simulation using NCODA to assimilate satellite SST and SSHA and in situ temperature and

salinity profiles. For the assimilation, the SSHA are extended into the ocean interior by adjusting the layer thickness as proposed by Cooper and Haines (1996). The mean Gulf Stream pathway in SSH from the "climatological" simulation is corrected by rubber sheeting the climatological mean SSH, which is added to the SSHA. The assimilation generates a mean Gulf Stream that follows the IR path from the coast out to 68°W, as seen in Figure 14c. East of 68°W, the flow diverts southward of the IR path, turning sharply northward and splitting as the Stream crosses the New England Seamount Chain (NESC) at 64°W. The SSH variability shown in Figure 17c reproduces all of the features found in the observed altimetric SSH variability shown in Figure 8, an expected result since these data are assimilated. The Eulerian mean core speed of the Gulf Stream at the separation point near Cape Hatteras is relatively weak at only 1.1 m sec^{-1}, compared to the non-assimilative simulations and observations. The assimilative Gulf Stream is much stronger to the east with Eulerian mean speeds of 0.8 m sec^{-1} at 70°W and 0.6 m sec^{-1} at 65°W. A surprising result is the strong abyssal circulation in the assimilative simulation shown in Figure 15c. The key abyssal currents at 72°W and 68.5°W are present with strengths of 10 cm sec^{-1} and 8 cm sec^{-1} respectively. The southward flow at 72°W is associated with a cyclonic gyre. The AMOC is stronger, with transport greater than 18 Sv, and much deeper than in the non-assimilative simulations. Despite a weaker Gulf Stream at Cape Hatteras, data assimilation generates a vigorous eddy field which drives a strong abyssal circulation.

4.4 MODAS data assimilation

The second data assimilative example starts on 1 June 2007, taking its initial condition from the Cooper-Haines hindcast. The assimilation is performed through NCODA with the SSHA extended into the ocean interior using synthetic profiles of temperature and salinity from MODAS. The mean Gulf Stream follows the IR path extremely well to the east past the NESC to 62°W, as shown in Figure 14d. The Eulerian mean core speed near Cape Hatteras is weak, only 1.0 m sec^{-1}. However, core speed is a maximum of 1.2 m sec^{-1} at 72°W and exceeds 0.65 m sec^{-1} at 65°W. The SSH variability reproduces the observed altimetric SSH variability (Figure 17d). The eddy driven abyssal circulation is strong, with the key southward abyssal currents exceeding 10 cm sec^{-1}. Each of the key currents is associated with a strong cyclonic gyre as shown in Figure 15d. The AMOC is the strongest, exceeding 20 Sv, and deepest of the four experiments. Assimilating the MODAS synthetic profiles appears to generate the most realistic Gulf Stream system with strong eddies along the entire path driving a strong abyssal circulation.

4.5 Comparison of model forecasts and data assimilation

The MODAS hindcasts, discussed in Section 4.4, were used to initialize a set of 48 14-day forecasts at approximately weekly intervals of the hindcast. The forecast skill of the HYCOM prediction system has been discussed in Hurlburt et al. (2008a, 2009) and Chassignet et al. (2009). The 1/12° global model forecasts significantly beat persistence out to 14 days. However, the skill of the forecasts is insignificant after about 10 days, with the median anomaly

correlation between the forecast and the analysis for SSH dropping below 0.6 at 10 days in the Gulf Stream region. We can compare the effect of the model dynamics on the forecasts by using the differences between the forecasted mean Gulf Stream and the analyses. In Figure 18 the mean velocities in layer 6 (~25m) and layers 27-29 (~3000 m to the bottom) from 48 forecasts are shown. The 5-day forecast has appreciable skill with a median SSHA correlation of 0.8, but the 14-day forecast has little skill. In the forecasts, we find significant changes in the upper layer flow, but only modest changes in the abyssal circulation. The 5-day forecast still tracks the mean IR path west of the NESC (64°W), but the core speeds have decreased by approximately 0.1 m sec^{-1} along the entire Stream. The core speeds in the 14-day forecast have decreased substantially with the speed at 72°W dropping below 0.8 m sec^{-1}. The path of the Gulf Stream is deflected slightly southward around 68.5°W, presumably steered southward by the strong southward abyssal current at 68.5°W. The AMOC (not shown) for the 14-day forecast is slightly weaker and shallower than either the 5-day forecast or analyses. The Gulf Stream in the forecasts is still inertial, with the variability driven by the instability of the flow. However, the dynamics of the model are insufficient to maintain a strong flow eastward to the NESC and the forecast Gulf Stream weakens over the 14-day period. The abyssal circulation appears to have a longer time scale showing little change in the mean over the 14-day forecast period. Thus, the steering by the abyssal currents helps to maintain a reasonable pathway, but the dynamics cannot maintain the strength of the Gulf Stream.

4.6 Discussion

Data assimilation provides a surprising change in the modeled behavior of the Gulf Stream. The non-assimilative simulations fail to generate a strong abyssal circulation and have a weak AMOC. The Gulf Stream path is poorly simulated without the steering by the abyssal circulation. Data assimilation forces the Gulf Stream to reproduce the pathway and SSH variability seen in the altimetric SSH. The mean currents of the Gulf Stream near the surface are weaker than the non-assimilative models, but extend much farther eastward with greater velocities. The eddies and meanders forced by the data assimilation drive a robust abyssal circulation reproducing the key currents identified by Hurlburt and Hogan (2008) and observed in the deep current meter records (Figures 5 and 6). The mean abyssal circulation is persistent over at least 14 days, which helps improve the character of the mean Gulf Stream in the forecasts compared to the non-assimilative models.

Acknowledgements

The US effort was supported by the US Global Ocean Data Assimilation Experiment (GODAE): Global Ocean Prediction with the HYbrid Coordinate Ocean Model (HYCOM) project, funded under the National Ocean Partnership Program (NOPP); by the 6.1 project Global Remote

Littoral Forcing via Deep Water Pathways, funded by the Office of Naval Research (ONR) under program element 601153N; and by grants of computer time from the US Defense Department High Performance Computing Modernization Program. The European high-resolution global ocean model was developed in France by Mercator Océan with the financial support of the European MERSEA integrated project for the development, validation, and exploitation of the system and from the Région Midi Pyrénées, which financed a dedicated computer for this project. The mean Gulf Stream northwall pathway, based on satellite infrared imagery, is an unpublished analysis performed by Peter Cornillon (University of Rhode Island) and Ziv Sirkes (deceased) for the ONR project Data Assimilation and Model Evaluation Experiment –North Atlantic Basin (DAMEE–NAB).

References

Barron CN, Smedstad LF, Dastugue JM, Smedstad OM (2007) Evaluation of ocean models using observed and simulated drifter trajectories: Impact of sea surface height on synthetic profiles for data assimilation. J Geophys Res 112:C07019 doi:10.1029/2006JC002982

Bleck R (2002) An oceanic general circulation model framed in hybrid isopycnic-cartesian coordinates. Ocean Model 37:55-88

Bleck R, Smith L (1990) A wind-driven isopycnic coordinate model of the north and equatorial Atlantic Ocean. 1. Model development and supporting experiments. J Geophys Res 95:3273-3285

Bower AS, Hunt HD (2000) Lagrangian observations of the Deep Western Boundary Current in the North Atlantic Ocean. Part II. The Gulf Stream—DeepWestern Boundary Current crossover. J Phys Oceanogr 30:784–804

Bryan FO, Hecht MW, Smith RD (2007) Resolution convergence and sensitivity studies with North Atlantic circulation models. Part I: The western boundary current system. Ocean Model 16:141-159

Chassignet EP, Marshall DP (2008) Gulf Stream separation in numerical ocean models. In: Hecht M, Hasumi H (eds) Ocean Modeling in an Eddying Regime, Geophysical Monograph 177. American Geophysical Union, Washington, DC

Chassignet EP, Hurlburt HE, Metzger EJ et al (2009) US GODAE: Global ocean prediction with the HYbrid Coordinate Ocean Model (HYCOM). Oceanogr 22:64-75

Cooper M, Haines KA (1996) Altimetric assimilation with water property conservation. J Geophys Res 24:1059–1077

Cummings JA (2005) Operational multivariate ocean data assimilation. Q J Roy Meteorol Soc 131:3583-3604

Fox DN, Teague WJ, Barron CN et al (2002) The Modular Ocean Data Analysis System (MODAS). J Atmos Ocean Technol 19:240-252

Godfrey JS (1989) A Sverdrup model of the depth-integrated flow for the world ocean allowing for island circulations. Geophys Astrophys Fluid Dyn 45:89-112

Halkin D, Rossby HT (1985) The structure and transport of the Gulf Stream at 73°W. J Phys Oceanogr 15:1439-1452

Haltiner GJ, Martin FL (1957) Dynamical and Physical Meteorology. McGraw-Hill, New York

Hecht MW, Smith RD (2008) Towards a physical understanding of the North Atlantic: A review of model studies in an eddying regime. In: Hecht M, Hasumi H (eds) Ocean Modeling in an Eddying Regime, Geophysical Monograph 177. American Geophysical Union, Washington, DC

Hecht MW, Hunke E, Maltrud ME et al (2008) Lateral mixing in the eddying regime and a new broad-ranging formulation. In: Hecht M, Hasumi H (eds) Ocean Modeling in an Eddying Regime, Geophysical Monograph 177. American Geophysical Union, Washington, DC

Hellerman S, Rosenstein M (1983) Normal monthly wind stress over the world ocean with error estimates. J Phys Oceanogr 13:1093–1104

Hogan PJ, Hurlburt HE (2006) Why do intrathermocline eddies form in the Japan/East Sea? A modeling perspective. Oceanography 19:134-143

Hogg NG, Stommel H (1985) On the relation between the deep circulation and the Gulf Stream. Deep-Sea Res 32:1181-1193

Hurlburt HE, Hogan PJ (2000) Impact of 1/8° to 1/64° resolution on Gulf Stream model-data comparisons in basin-scale subtropical Atlantic Ocean models. Dyn Atmos Ocean 32:283-329

Hurlburt HE, Hogan PJ (2008) The Gulf Stream pathway and the impacts of the eddy-driven abyssal circulation and the Deep Western Boundary Current. Dyn Atmos Ocean 45:71-101

Hurlburt HE, Thompson JD (1980) A numerical study of Loop Current intrusions and eddy shedding. J Phys Oceanogr 10:1611-1651

Hurlburt HE, Thompson JD (1982) The dynamics of the Loop Current and shed eddies in a numerical model of the Gulf of Mexico. In: Nihoul JCJ (Ed) Hydrodynamics of Semi-Enclosed Seas, Elsevier, Amsterdam

Hurlburt HE, Wallcraft, AJ, Schmitz Jr WJ et al (1996) Dynamics of the Kuroshio/Oyashio current system using eddy-resolving models of the North Pacific Ocean. J Geophys Res 101(C1): 941–976

Hurlburt HE, Chassignet EP, Cummings JA et al (2008a) Eddy resolving global ocean prediction. In: Hecht M, Hasumi H (ed) Ocean Modeling in an Eddying Regime Geophysical Monograph 177 American Geophysical Union, Washington, DC

Hurlburt HE, Metzger EJ, Hogan PJ et al (2008b) Steering of upper ocean currents and fronts by the topographically constrained abyssal circulation. Dyn Atmos Ocean 45:102-134, doi:10.1016/j.dynatmoce.2008.06.003

Hurlburt HE, Brassington GB, Drillet Y et al (2009) High-resolution global and basin-scale ocean analyses and forecasts. Oceanogr 22:110-127

Johns WE, Shay TJ, Bane JM et al (1995) Gulf Stream structure, transport, and recirculation near 68°W. J Geophys Res 100:817-838

Joyce TM, Wunsch C, Pierce SD (1986) Synoptic Gulf Stream velocity profiles through simultaneous inversion of hydrographic and acoustic Doppler data. J Geophys Res 91:7573-7585

Kara AB, Wallcraft AJ, Martin PJ, Pauley RL (2009) Optimizing surface winds using QuikSCAT measurements in the Mediterranean Sea during 2000-2006. J Mar Sys 78:119-131

Lee H (1997) A Gulf Stream synthetic geoid for the TOPEX altimeter. MS Thesis Rutgers University, New Brunswick, NJ

Madec G (2008) NEMO ocean engine. Report 27 ISSN No 1288-1619. Institute Pierre-Simon Laplace (IPSL), France

Munk WH (1950) On the wind-driven ocean circulation. J Met 7:79-93

Paiva AM, Hargrove JT, Chassignet EP, Bleck R (1999) Turbulent behavior of a fine mesh (1/12°) numerical simulation of the North Atlantic. J Mar Sys 21:307-320

Pickart RS (1994) Interaction of the Gulf Stream and Deep Western Boundary Current where they cross. J Geophys Res 99:25155-25164

Pickart RS, Watts DR (1990) Deep Western Boundary Current variability at Cape Hatteras. J Mar Res 48:765-791

Reid RO (1972) A simple dynamic model of the Loop Current. In: Capurro LRA, Reid JL (eds) Contributions on the Physical Oceanography of the Gulf of Mexico. Gulf Publishing Co, Houston, TX

Rossby CG (1940) Planetary flow patterns in the atmosphere. Q J Roy Meteorol Soc 66:68-87

Rossby T, Flagg CN, Donohue K (2005) Interannual variations in upper-ocean transport by the Gulf Stream and adjacent waters between New Jersey and Bermuda. J Mar Res 63:203-226

Smedstad OM, Hurlburt HE, Metzger EJ et al (2003) An operational eddy resolving 1/16° global ocean nowcast/forecast system. J Mar Sys 40-41:341-361

Schmitz WJ Jr (1996) On the world ocean circulation: Volume I. Some global features/North Atlantic circulation. Technical Report WHOI-96-03 Woods Hole Oceanographic Institution, Woods Hole, MA

Schmitz WJ Jr, McCartney MS (1993) On the North Atlantic circulation. Rev Geophys 31:29-49

Smith RD, Maltrud ME, Bryan FO, Hecht MW (2000) Numerical simulation of the North Atlantic Ocean at 1/10°. J Phys Oceanogr 30:1532-1561

Sverdrup HU (1947) Wind-driven currents in a baroclinic ocean – with application to the equatorial currents of the eastern Pacific. Proc Natl Acad Sci USA 33:318-326

Thompson JD, Schmitz WJ Jr (1989) A regional primitive-equation model of the Gulf Stream: Design and initial experiments. J Phys Oceanogr 19:791-814

Townsend TL, Hurlburt HE, Hogan PJ (2000) Modeled Sverdrup flow in the North Atlantic from 11 different wind stress climatologies. Dyn Atmos Oceans 32:373-417

Tsujino H, Usui N, and Nakano H (2006) Dynamics of Kuroshio path variations in a high-resolution general circulation model. J Geophys Res. doi:10.1029/2005JC003118

Usui N, Tsujino H, Fujii Y (2006) Short-range prediction experiments of the Kuroshio path variabilities south of Japan. Ocean Dyn 56:607-623

Usui N, Tsujino H, Fujii Y, Kamachi M (2008a) Generation of a trigger meander for the 2004 Kuroshio large meander. J Geophys Res. doi:10.1029/2007JC004266

Usui N, Tsujino H, Nakano H, Fujii Y (2008b) Formation process of the Kuroshio large meander in 2004. J Geophys Res. doi:10.1029/2007JC004675

Watts DR, Tracey KL, Bane JM, Shay TJ (1995) Gulf Stream path and thermocline structure near 74°W and 68°W. J Geophys Res 100:18291-18312

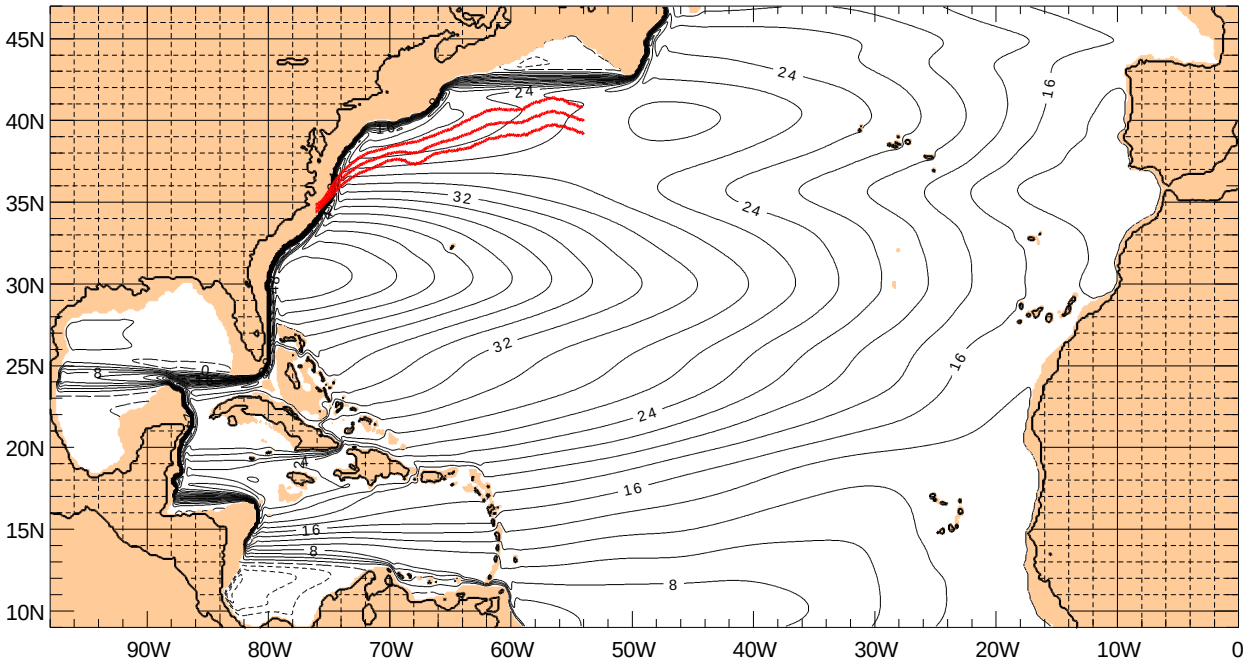

Fig. 1. Mean transport streamfunction (Ψ) from a 1/16°, 1.5-layer linear reduced-gravity simulation forced by the smoothed Hellerman and Rosenstein (1983) wind stress climatology and the northward upper ocean flow (14 Sv) of the Atlantic meridional overturning circulation (AMOC), forcing used for all of the simulations in Section 2. The mean Gulf Stream IR northwall pathway $\pm$ 1σ from Cornillon and Sirkes is overlaid. The contour interval is 2 Sv. The streamfunction shown here covers the 9°-47°N model domain used by all the nonlinear simulations discussed in Section 2. [from Hurlburt and Hogan, 2008, as adapted from Townsend et al., 2000]

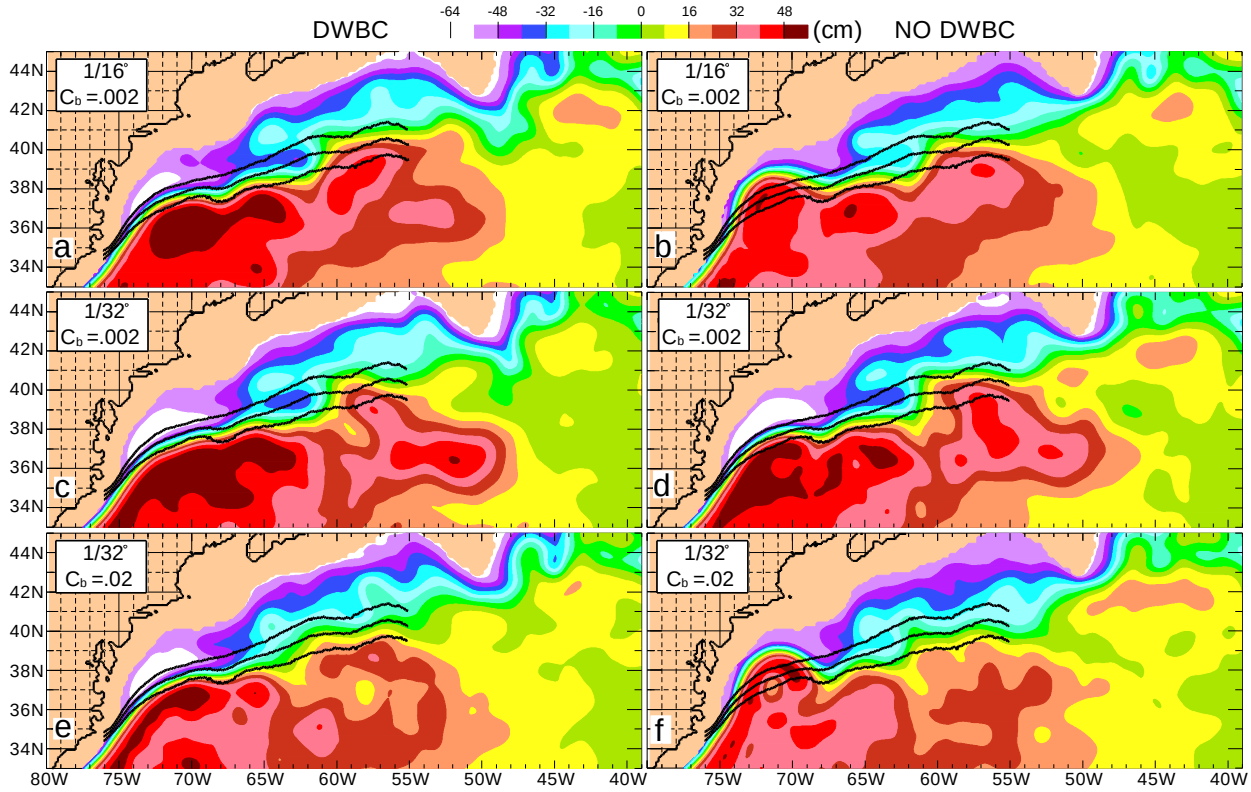

Fig. 2. Mean SSH from six 5-layer Atlantic Ocean simulations (9°-47°N), including the Intra-Americas Sea, zoomed into the Gulf Stream region between Cape Hatteras and the Grand Banks. The simulations depicted in (a), (c) and (e) include a DWBC while those in (b), (d) and (f) do not. (a) and (b) depict results from 1/16° simulations with ~7 km mid-latitude resolution for each variable, (c-f) from corresponding 1/32° simulations, (a-d) with a coefficient of quadratic bottom friction, C_b = .002, (d) and (f) with a 10x increase to C_b = .02. The northward upper ocean flow of the AMOC is included in all six simulations. The Laplacian coefficient of isopycnal eddy viscosity is A = 20 m^2sec^{-1} for the 1/16º simulations and A = 10 m^2sec^{-1} for the 1/32º simulations. The SSH contour interval is 8 cm. The mean Gulf Stream IR northwall pathway $\pm 1\sigma$ from Cornillon and Sirkes is overlaid on each panel. For more information about the simulations used in Section 2, see Hurlburt and Hogan (2008). [From Hurlburt and Hogan, 2008]

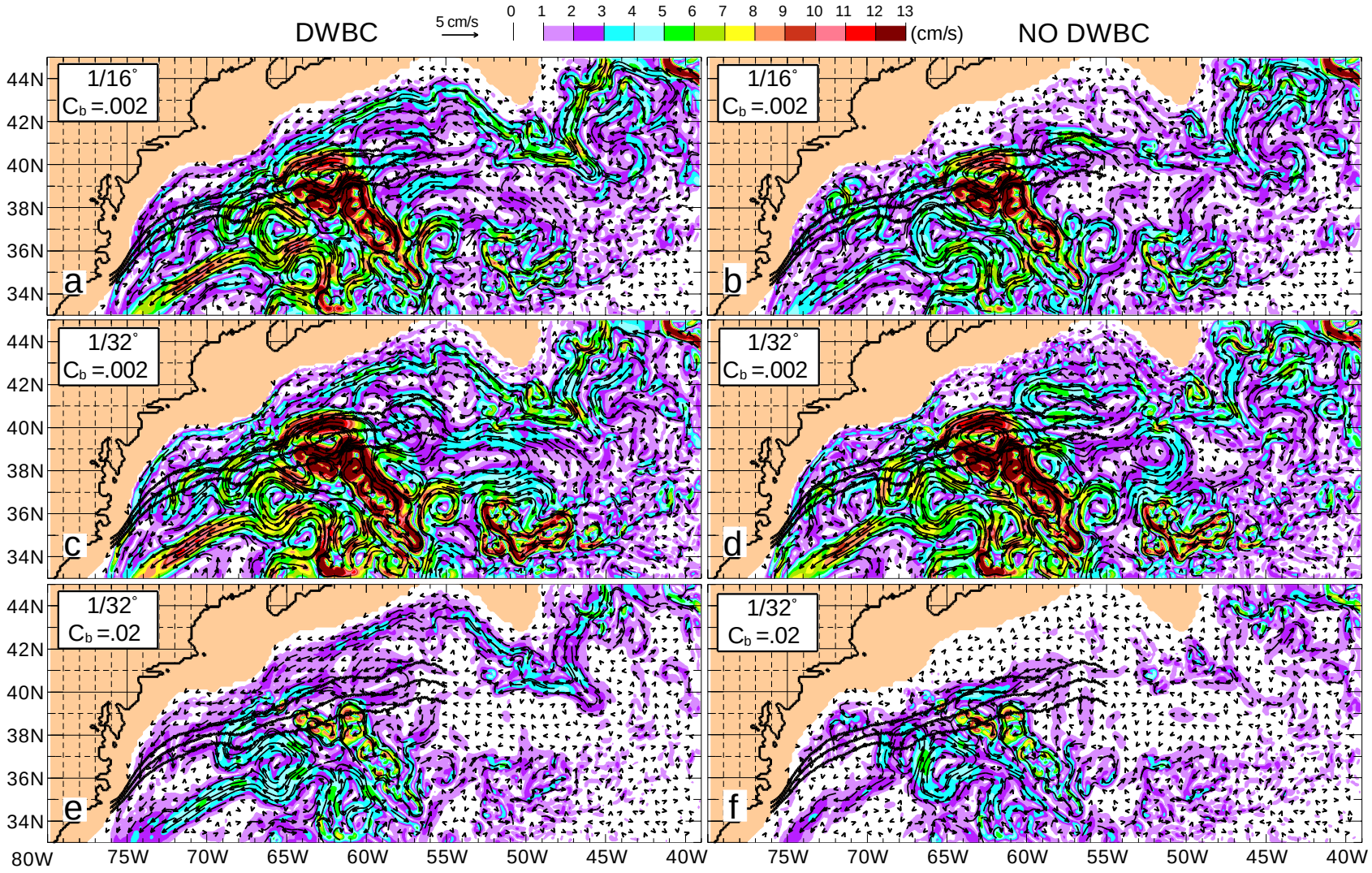

Fig. 3. Same as Fig. 2 except for mean abyssal currents (arrows) overlaid on isotachs (in cm s^{-1}). The DWBC is most easily seen paralleling the northern model boundary north of 41°N between 65°W and 51°W in panels (a,c,e). In the simulations with no DWBC (panels b,d,f) that current is not present. [From Hurlburt and Hogan, 2008]

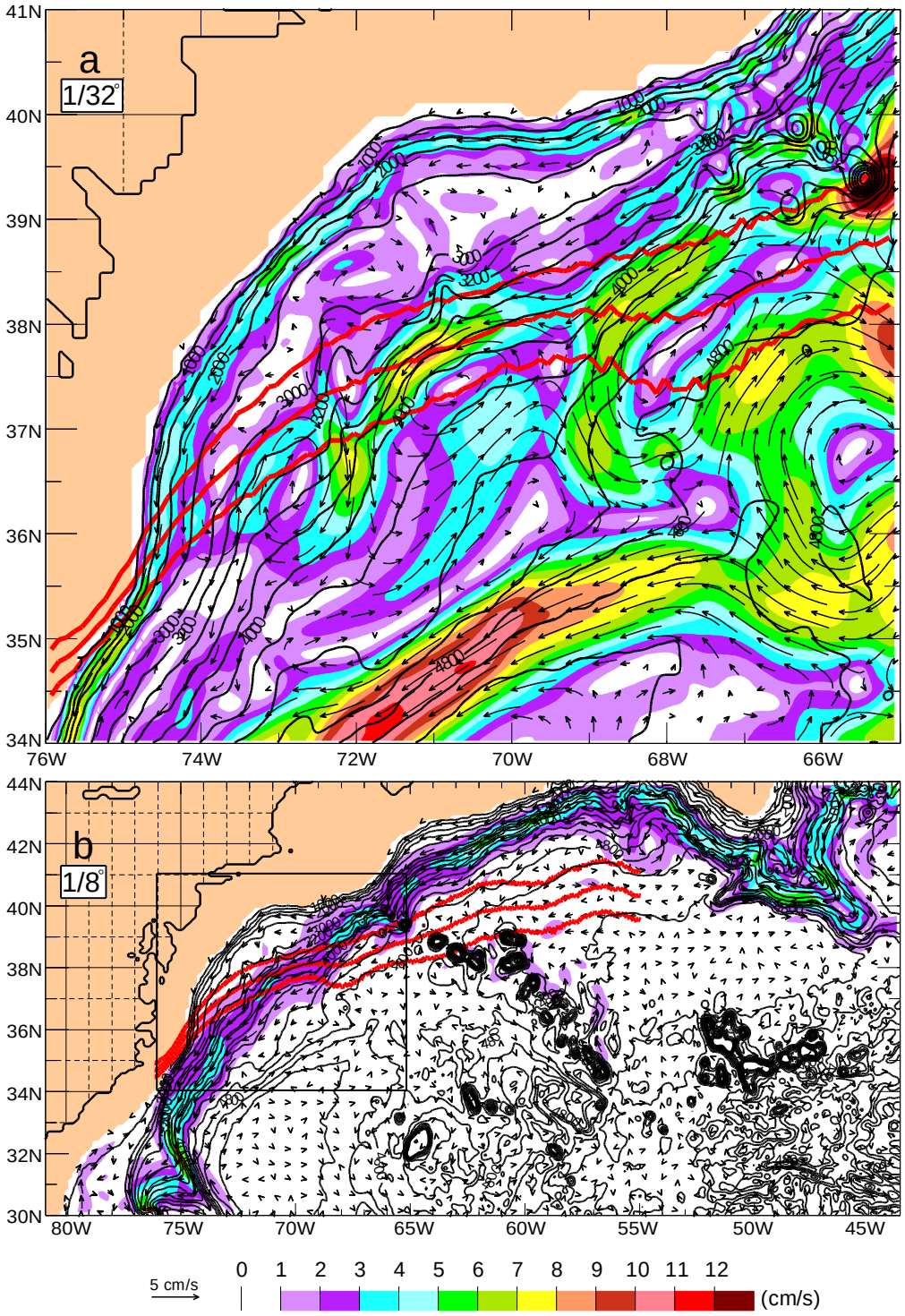

Fig. 4. (a) Zoom of Fig. 3c with (full amplitude, uncompressed) depth contours (in m) overlaid to facilitate geographical co-location in the model-data comparisons. (b) Same as (a) but covering a larger region from a corresponding 1/8° simulation overlaid with a box outlining the region covered by (a). In the 1/8º simulation A = 100 $m^2 sec^{-1}$ and C_b = .002. [From Hurlburt and Hogan, 2008]

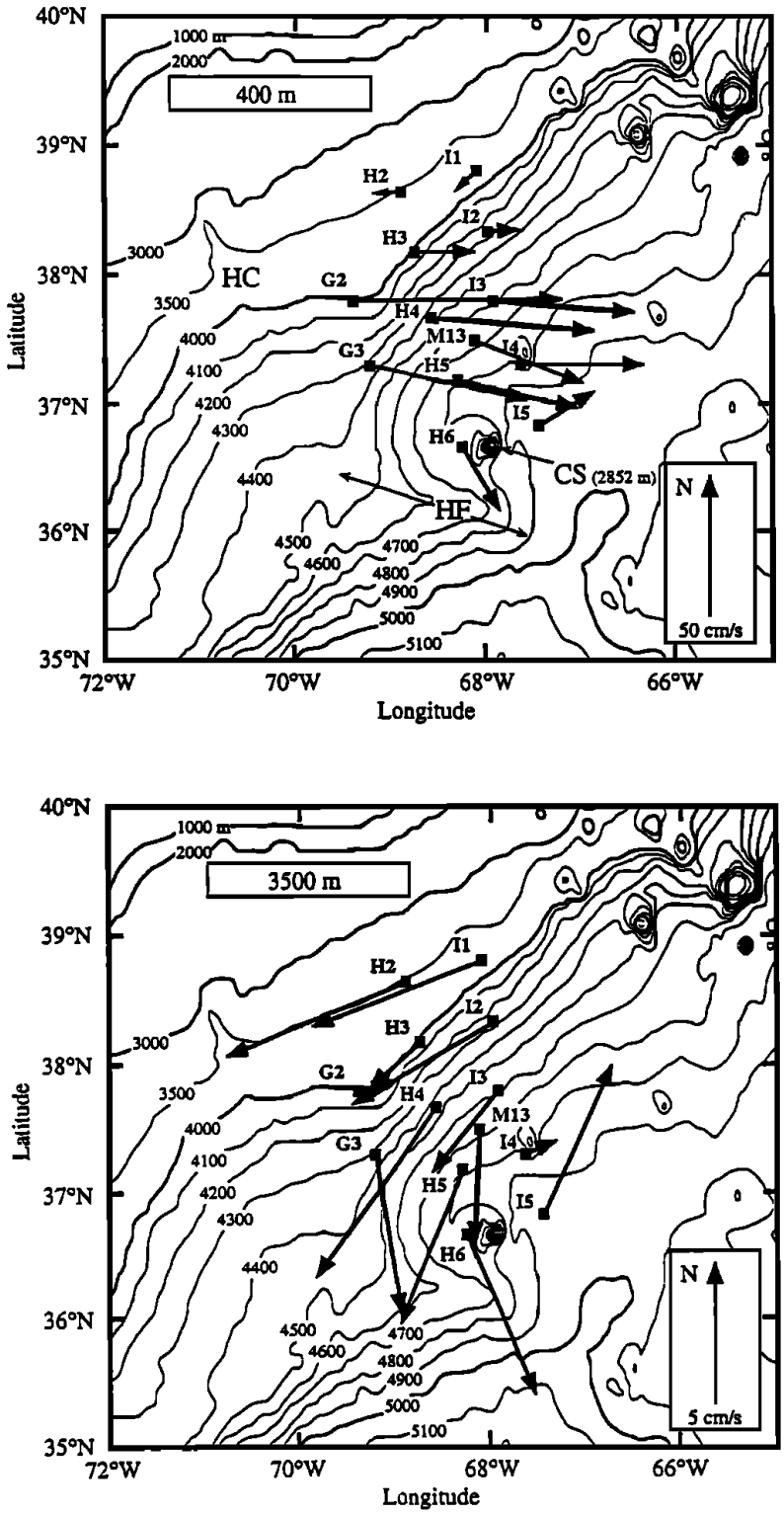

Fig. 5. Mean current meter velocities at 400 m (top) and 3500 m (bottom) over the entire deployment, June 1988 - August 1990. All of the vectors represent 26-month means except at sites H5 and M13, which are approximately 1-year means. [From Johns et al., 1995]

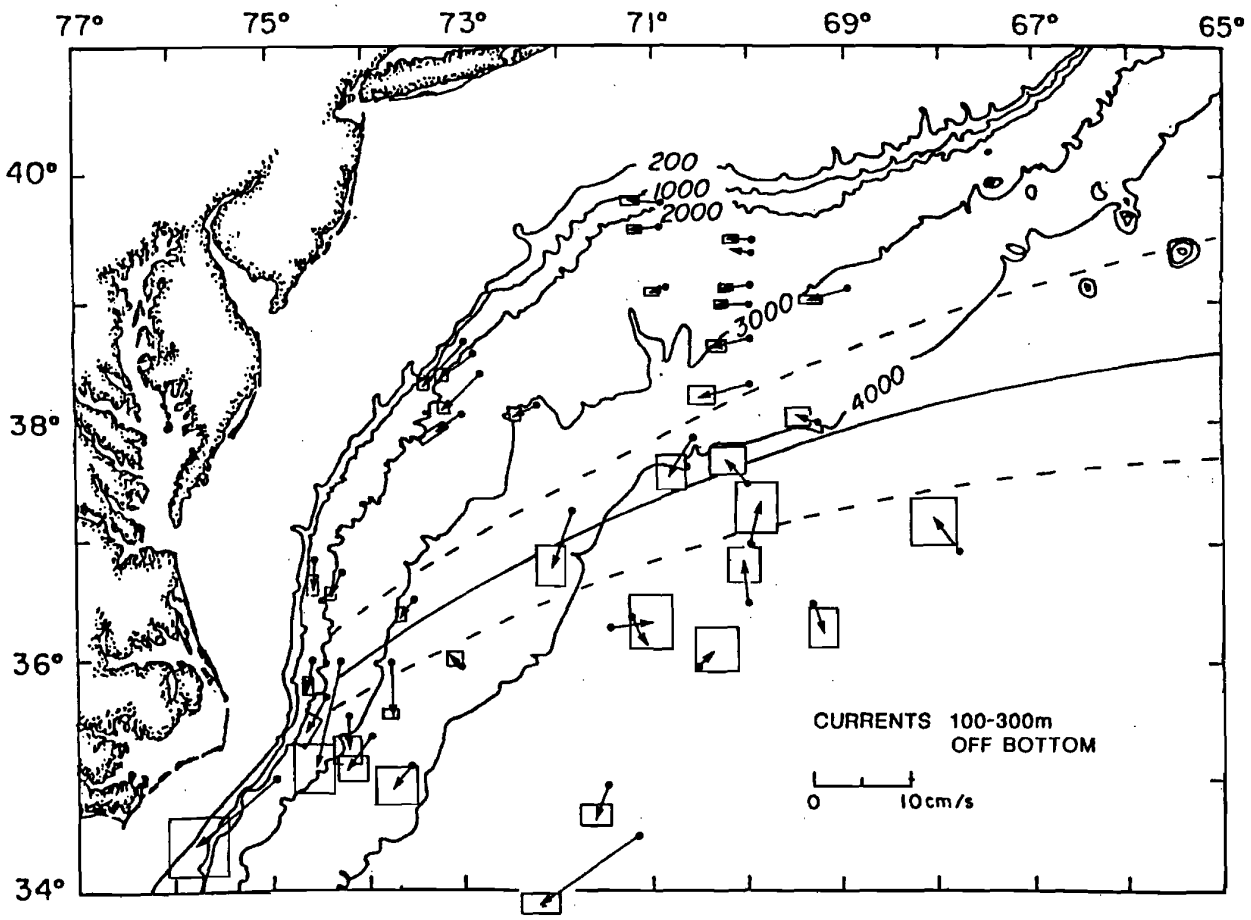

Fig. 6. Mean current meter velocities 100 - 300 m above the bottom from historical measurements collected in the middle Atlantic Bight. The record lengths of the measurements vary from 4 months to 2 years, and the box associated with each vector represents the uncertainty of the mean, typically 1 - 2 cm sec^{-1}. [From Pickart and Watts, 1990]

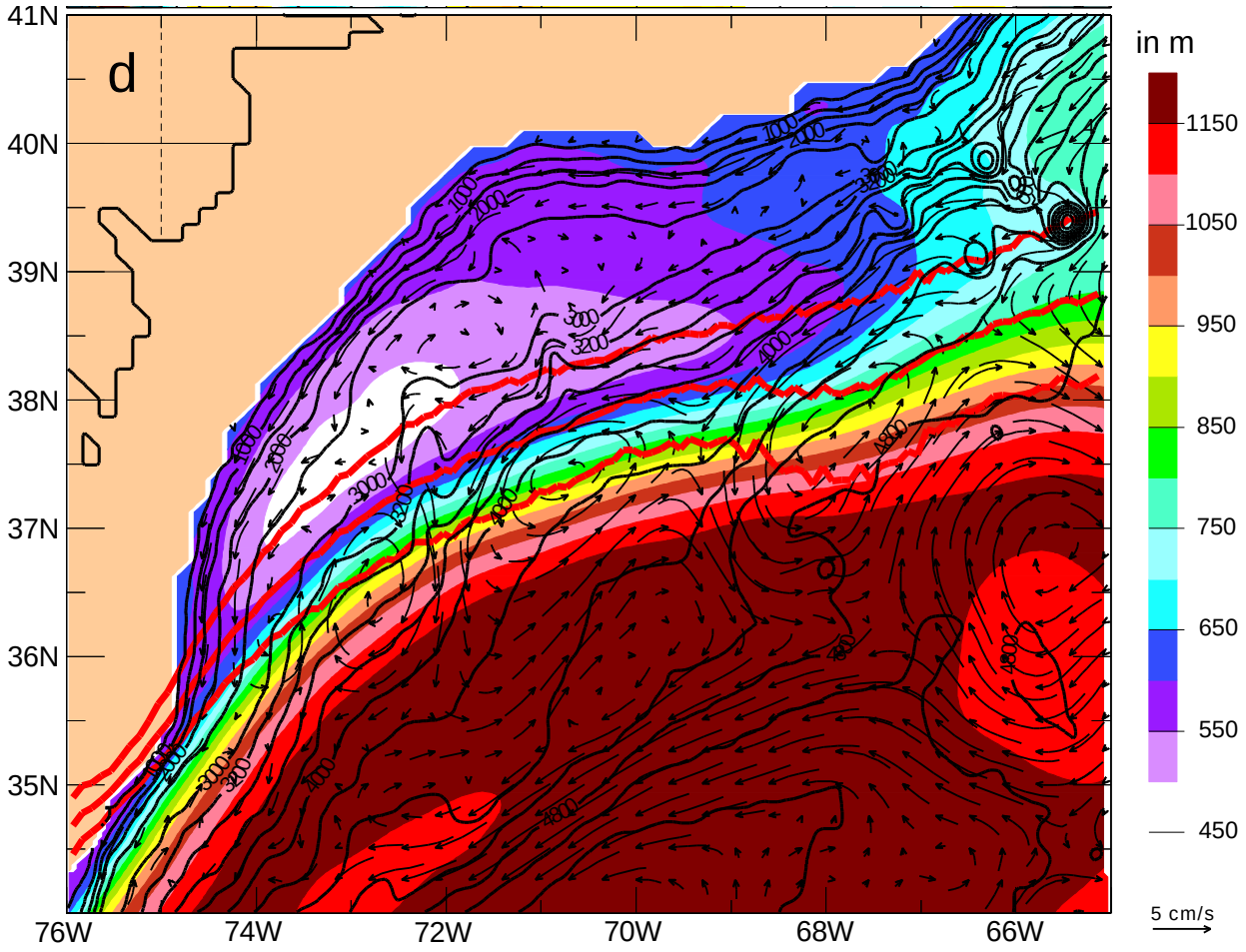

Fig. 7. Same as Fig. 4a but with isotachs (in color) replaced by the mean depth at the base of the model thermocline (in m) from the same simulation (in color), i.e. the mean depth of the interface between layer 4 and layer 5 (the abyssal layer) from the 1/32º simulation depicted in Figs. 2c and 3c. [From Hurlburt and Hogan, 2008]

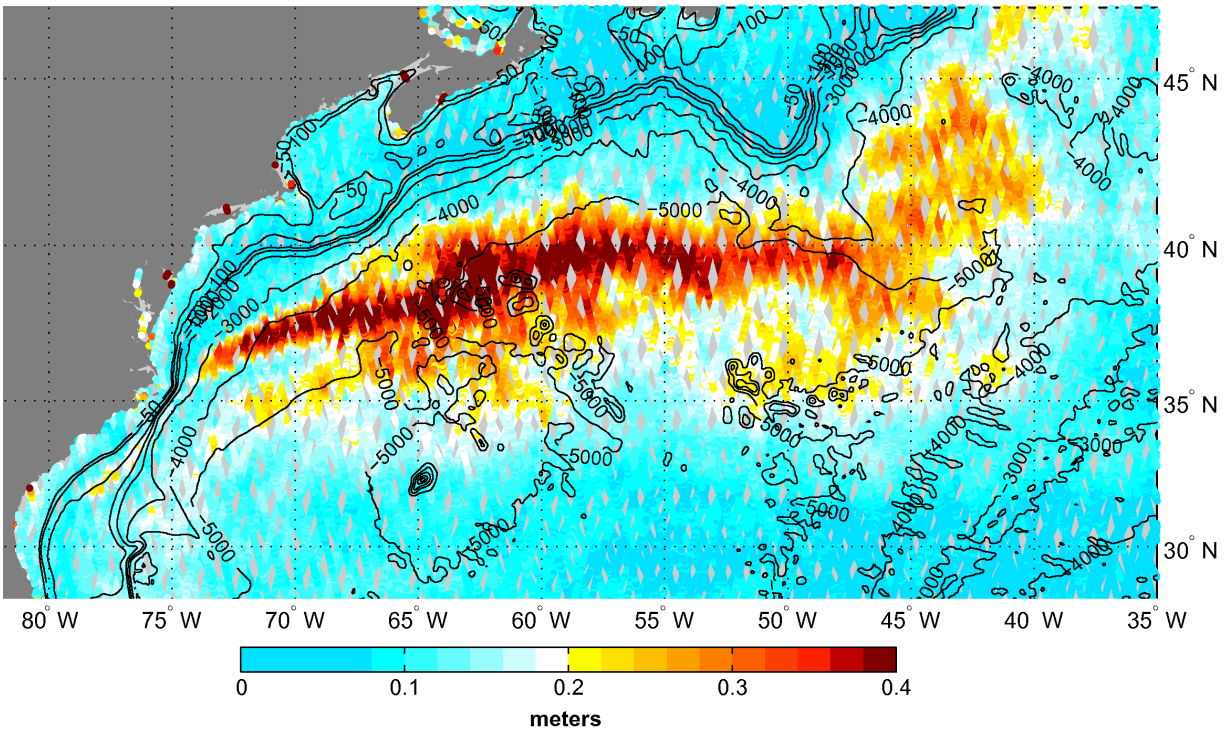

Fig. 8. Along-track SSH variability from quasi-contemporaneous satellite altimeter data in 4 different orbits overlaid on topographic contours (depth in m), Jason-1 over the period 15 Jan. 2002 –18 Oct. 2007, GFO over 15 July 1999 – 12 Dec. 2007, Envisat over 24 Sept. 2002 – 29 Oct. 2007, and Topex in an interleaved orbit over 16 Sept. 2002 – 8 Oct. 2005. The tracks are overlaid in the following order from top to bottom: (1) Envisat, (2) GFO, (3) Jason-1, and (4) Topex interleaved. (Provided by Gregg Jacobs, NRL) [From Hurlburt and Hogan, 2008]

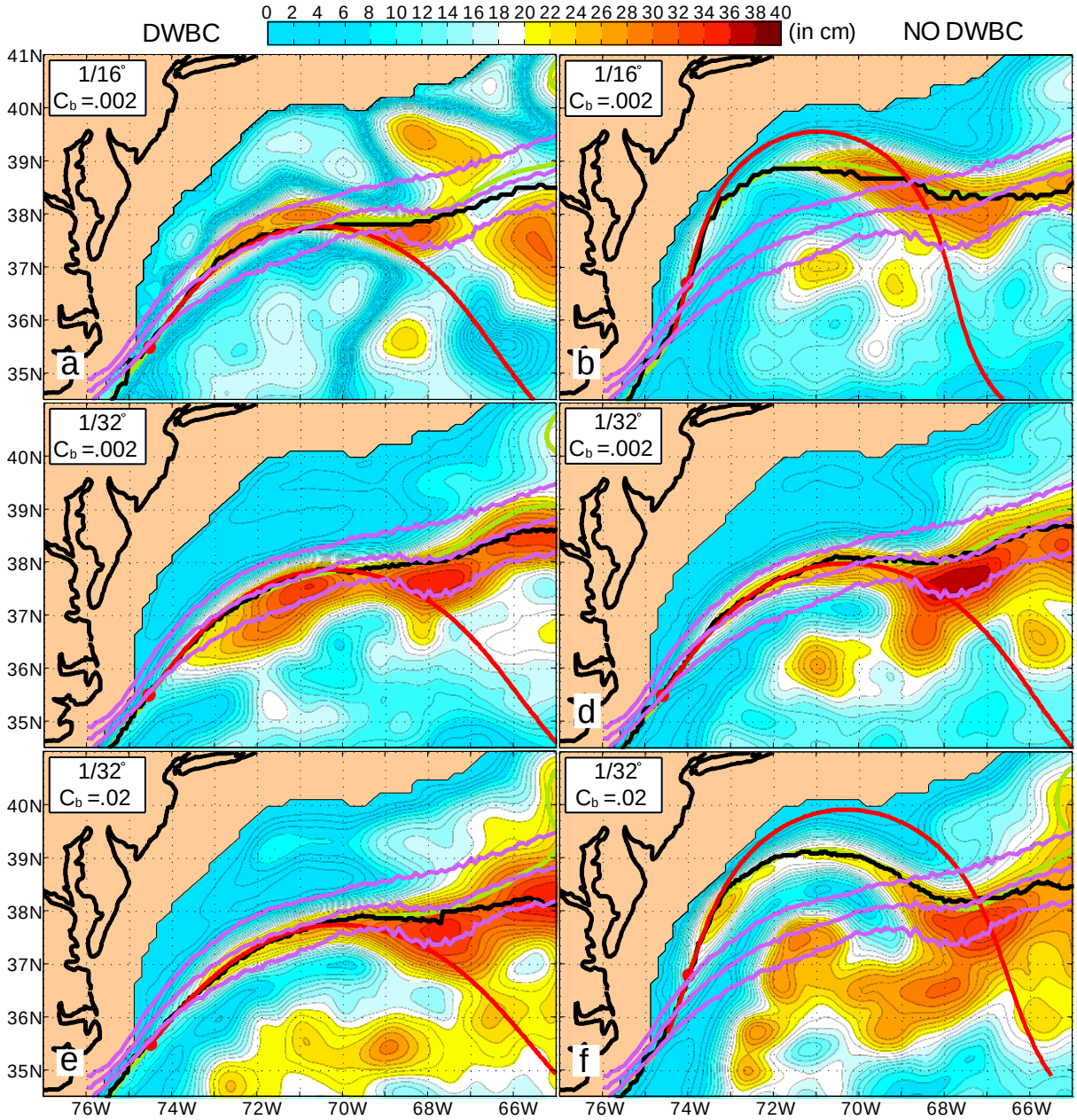

Fig. 9. CAV trajectory analysis for Gulf Stream pathways simulated by the six simulations illustrated in Fig. 2. The pathway of the maximum velocity at core of the current (black line), the closest SSH contour (yellow-green line), the corresponding CAV trajectory (red line with a circle at the inflection point), the observed IR northwall frontal pathway ± std. dev. (violet lines), and the simulated SSH variability are overlaid on each panel. Due to the hierarchy of the overlaid lines (light violet, red, black, yellow-green from top to bottom), lines on the bottom tend to be obscured where close agreement occurs. That is particularly the case for the yellow-green SSH contour west of ~68°W, where the core of the current overlaying a single SSH contour is a prerequisite for the existence of a CAV trajectory. The SSH contour closest to the pathway of the velocity maximum is skewed toward the north side of the model Gulf Stream as depicted in SSH and is (a) -24 cm, (b) -16 cm, (c) -28 cm, and (d-f) -24 cm. See the corresponding panels in Fig. 2. Near the western boundary the Gulf Stream axis from Topex/Poseidon altimetry (Lee, 1997) diverges from the IR frontal pathway in accord with the model simulations of panels a, c, d, and e (see Hurlburt and Hogan, 2000, their Fig. 7). [From Hurlburt and Hogan, 2008]

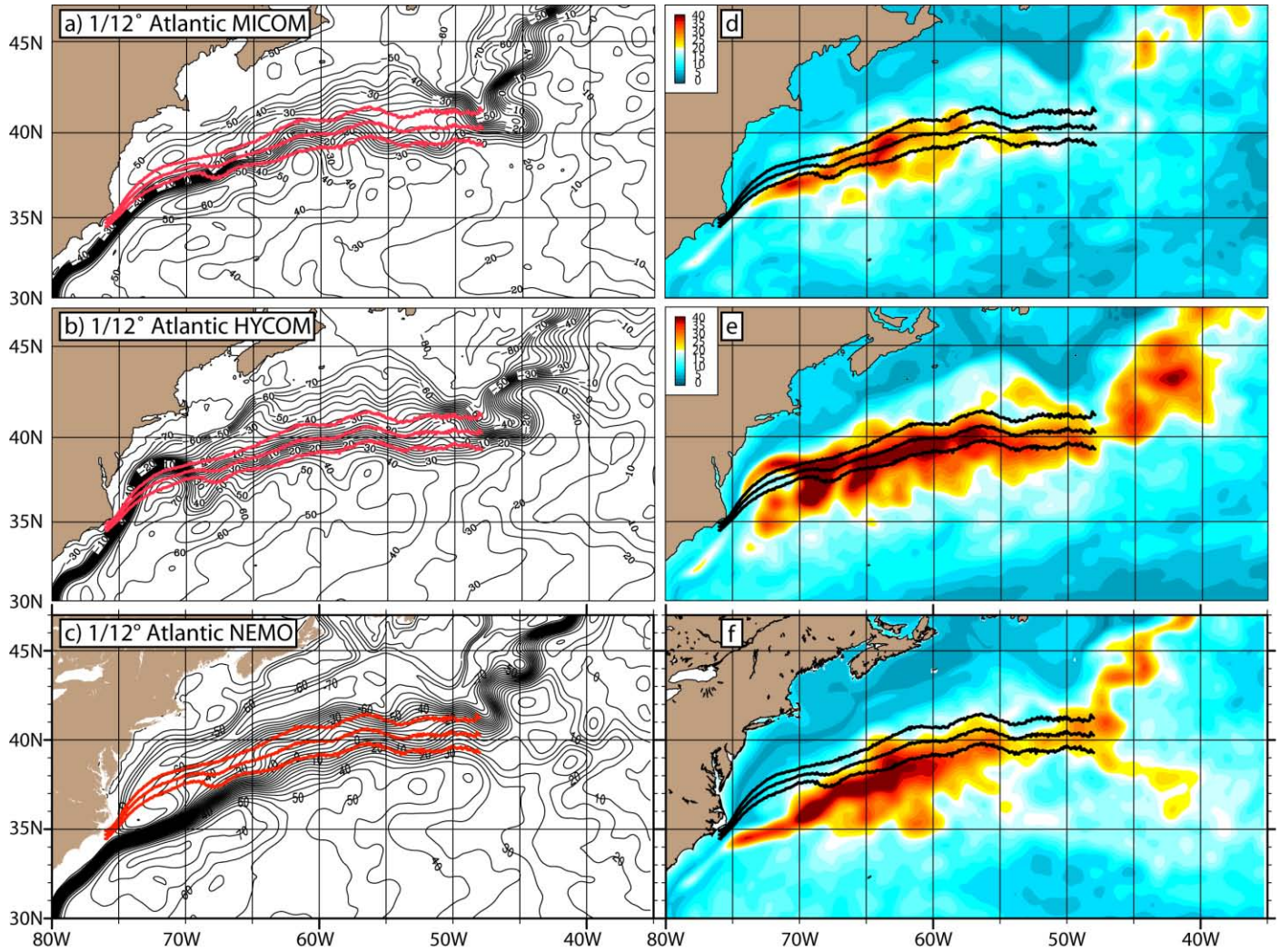

Fig. 10. Mean SSH (left column) and mean SSH variability (right column) from (a,d) a 1/12° Atlantic MICOM simulation over 1982-1983, (b,d) a 1/12° Atlantic HYCOM simulation over years 11-13, and (c,f) a 1/12° Atlantic NEMO simulation over 2004-2006. The contour interval in both columns is 5 cm. The mean Gulf Stream IR northwall pathway ± 1σ from Cornillon and Sirkes is overlaid on each panel in red in the left column and black in the right column.

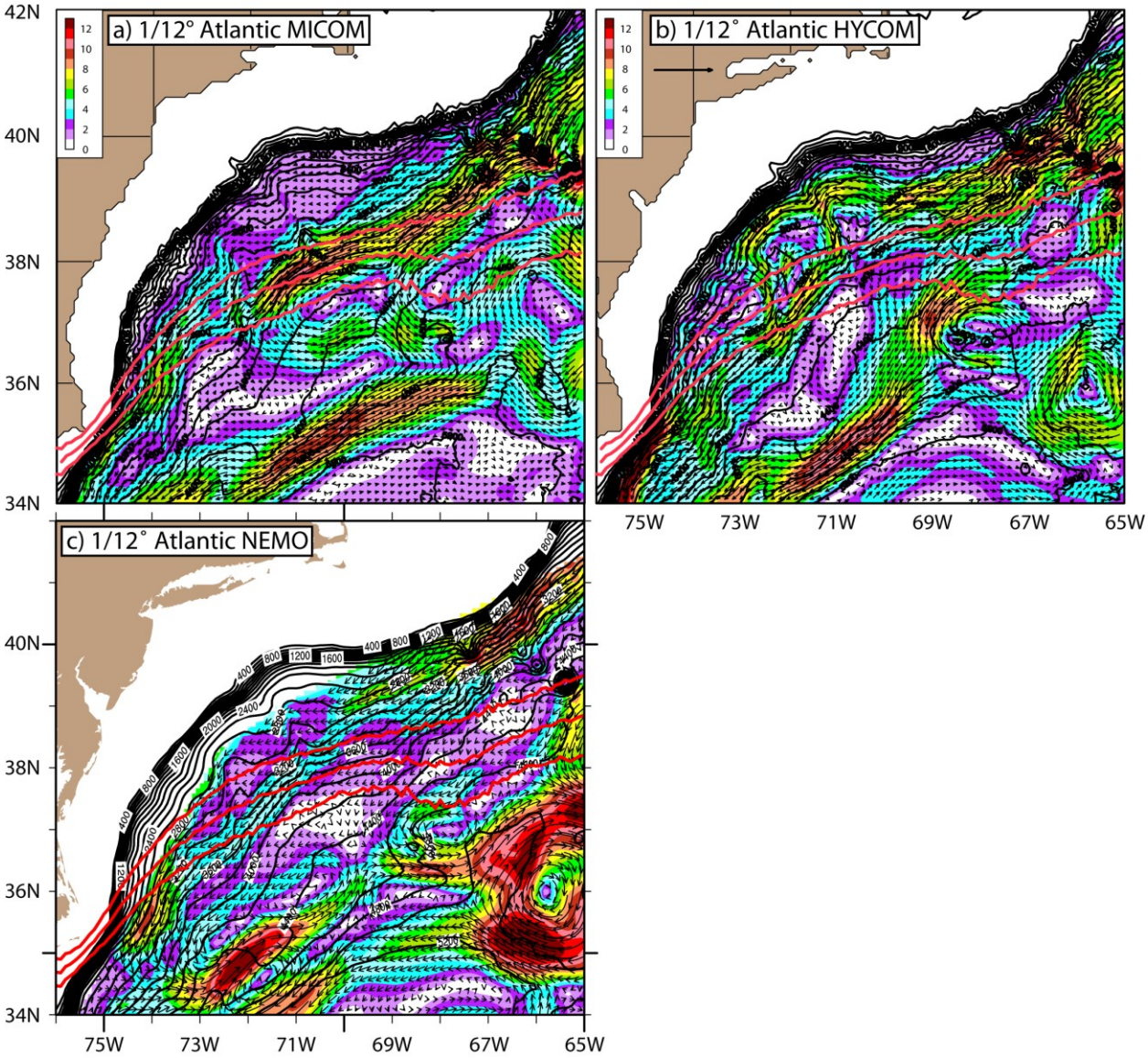

Fig. 11. Mean abyssal currents (arrows) overlaid on isotachs (in color with a 1 cm sec^{-1} contour interval) and topographic contours at intervals of 200 m from (a) 1/12° Atlantic MICOM, (b) 1/12° Atlantic HYCOM, and (c) 1/12° Atlantic NEMO. The reference vector length for the currents (black arrow over land in panel b) is 25 cm sec^{-1}. The mean Gulf Stream northwall pathway ± 1σ from Cornillon and Sirkes is overlaid in red on each panel.

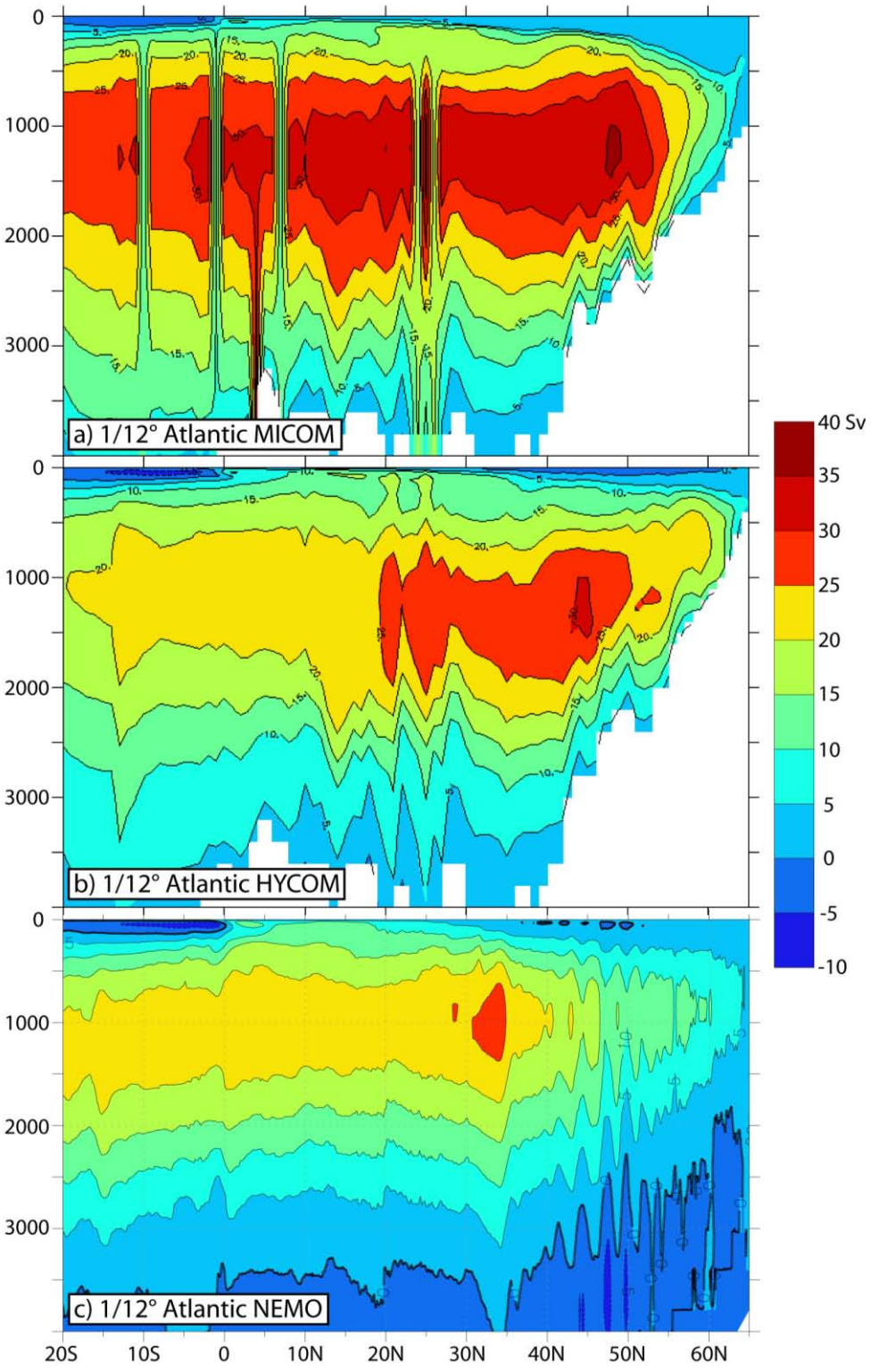

Fig. 12. Atlantic meridional overturning circulation (AMOC) streamfunction with a 5 Sv contour interval from (a) 1/12° Atlantic MICOM, (b) 1/12° Atlantic HYCOM, and (c) 1/12° Atlantic NEMO.

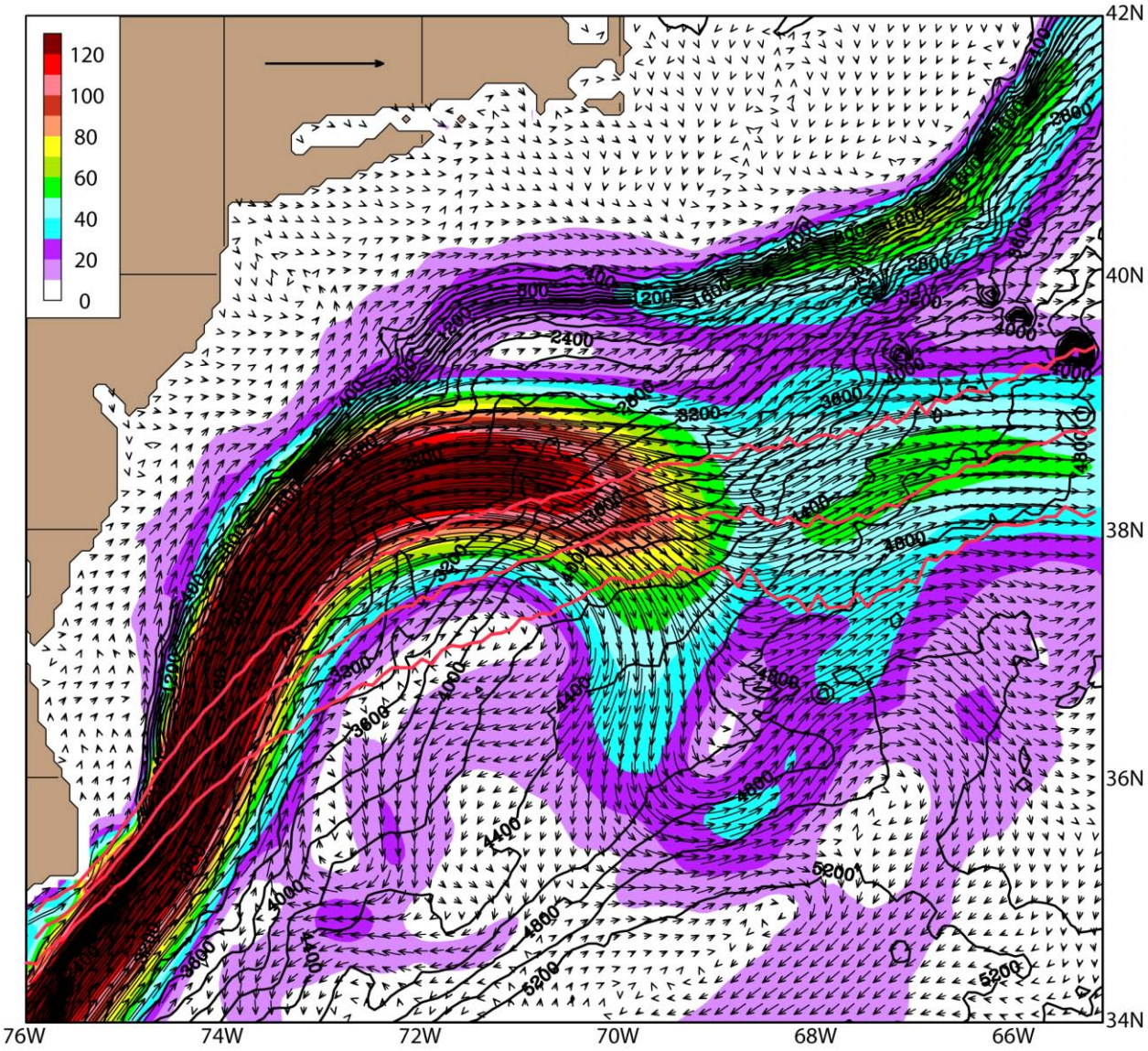

Fig. 13. Mean currents at the depth of the current core (~25 m in depth) overlaid on isotachs (in color with a 10 cm sec^{-1} contour interval) and topographic contours at intervals of 200 m from 1/12° Atlantic HYCOM. The mean Gulf Stream northwall pathway ± 1σ from Cornillon and Sirkes is overlaid in red. The reference vector length for the currents (black arrow over land) is 100 cm sec^{-1}.

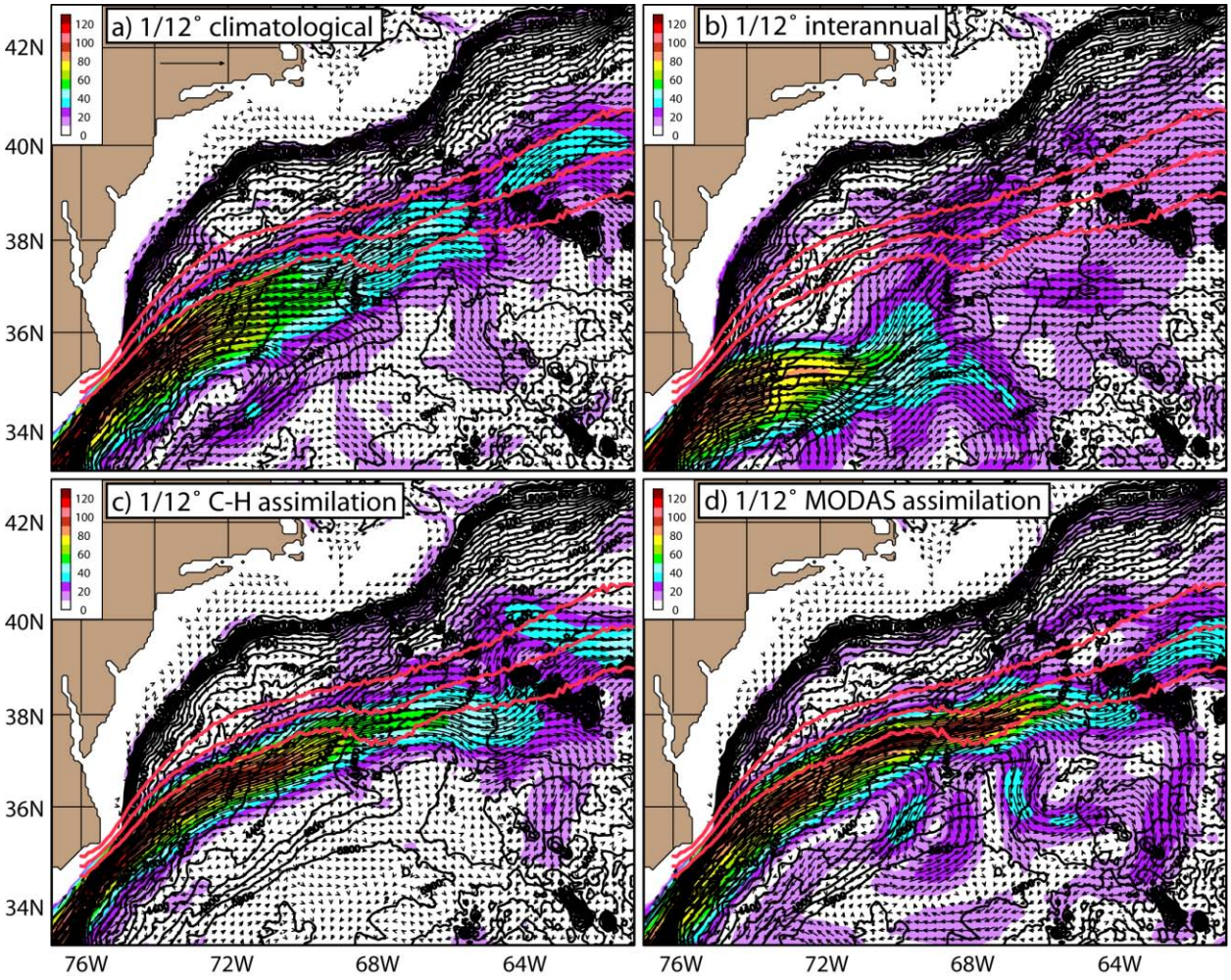

Fig. 14. Mean velocities in layer 6, approximately 25 m, with the 15-year mean Gulf Stream northwall pathway ± 1σ from Cornillon and Sirkes overlaid in red and the bathymetry contoured at 200 m intervals from four 1/12° global HYCOM simulations: (a) the ECMWF climatology forcing; (b) NOGAPS interannual forcing; (c) Cooper-Haines (1996) data assimilation with NOGAPS forcing and (d) MODAS synthetic temperature and salinity profile data assimilation with NOGAPS forcing.

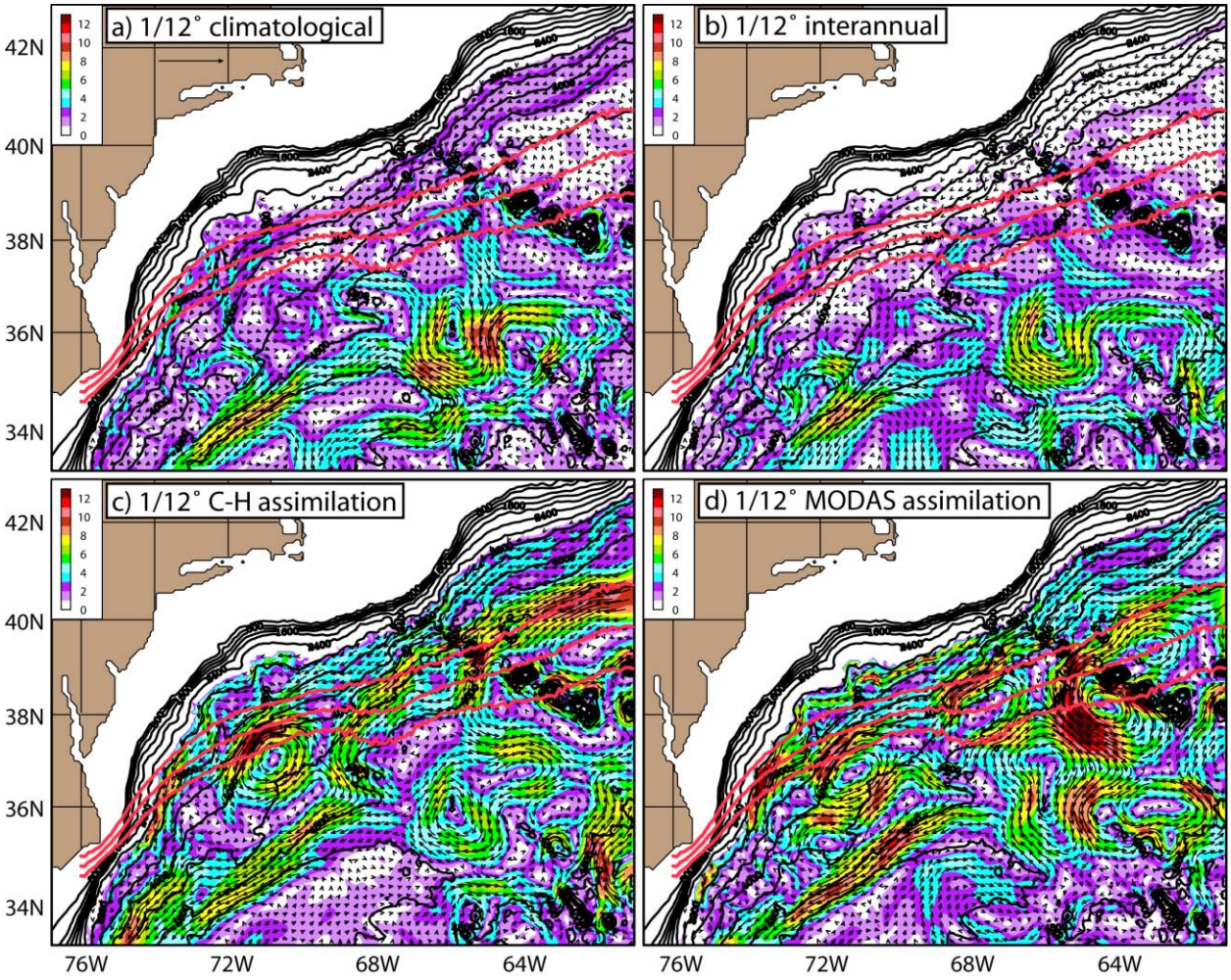

Fig. 15. Mean depth averaged velocities in layers 27 to 29, below approximately 3000 m depth, with the 15-year mean Gulf Stream northwall pathway ± 1σ from Cornillon and Sirkes overlaid in red and the bathymetry contoured at 200 m intervals from four 1/12° global HYCOM simulations: (a) the ECMWF climatology forcing; (b) NOGAPS interannual forcing; (c) Cooper-Haines (1996) data assimilation with NOGAPS forcing and (d) MODAS synthetic temperature and salinity profile data assimilation with NOGAPS forcing.

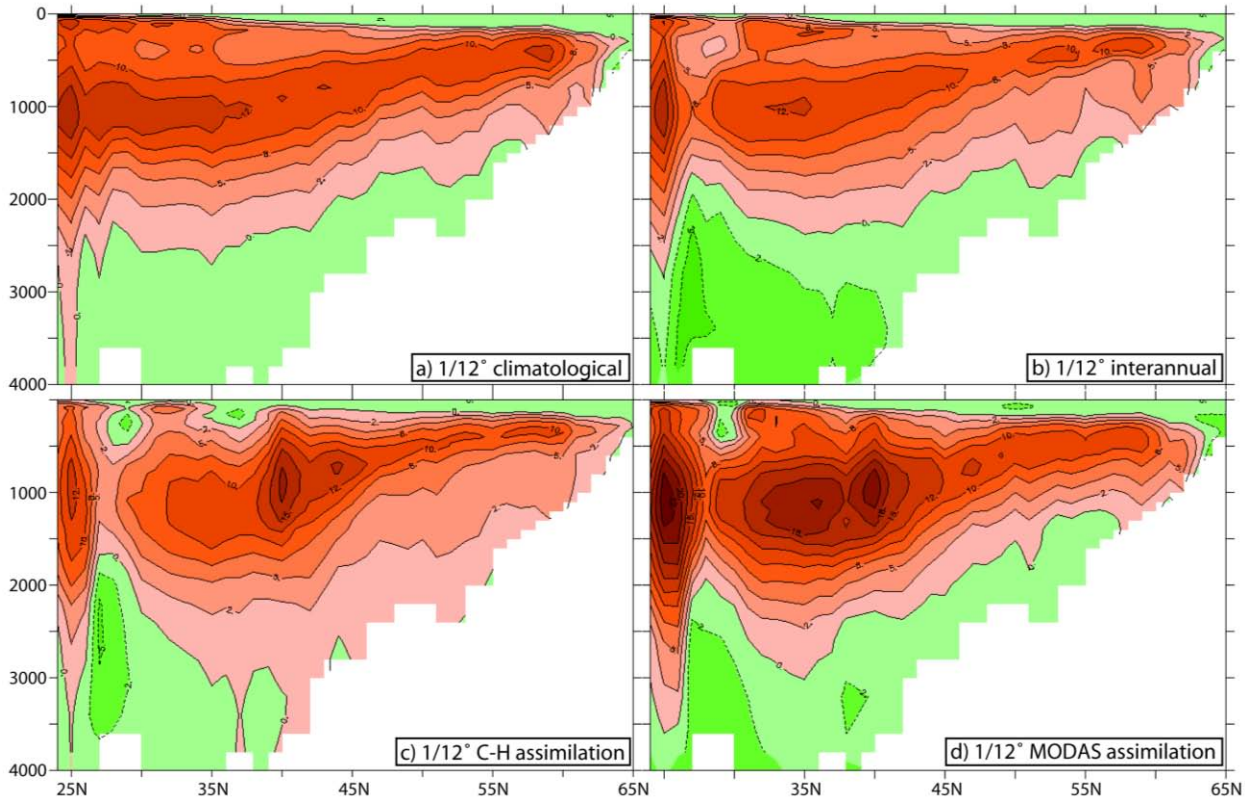

Fig. 16. Meridional overturning circulation streamfunction for the Atlantic north of 24°N (AMOC) from four 1/12° global HYCOM simulations: (a) the ECMWF climatology forcing; (b) NOGAPS interannual forcing; (c) Cooper-Haines (1996) data assimilation with NOGAPS forcing and (d) MODAS synthetic temperature and salinity profile data assimilation with NOGAPS forcing.

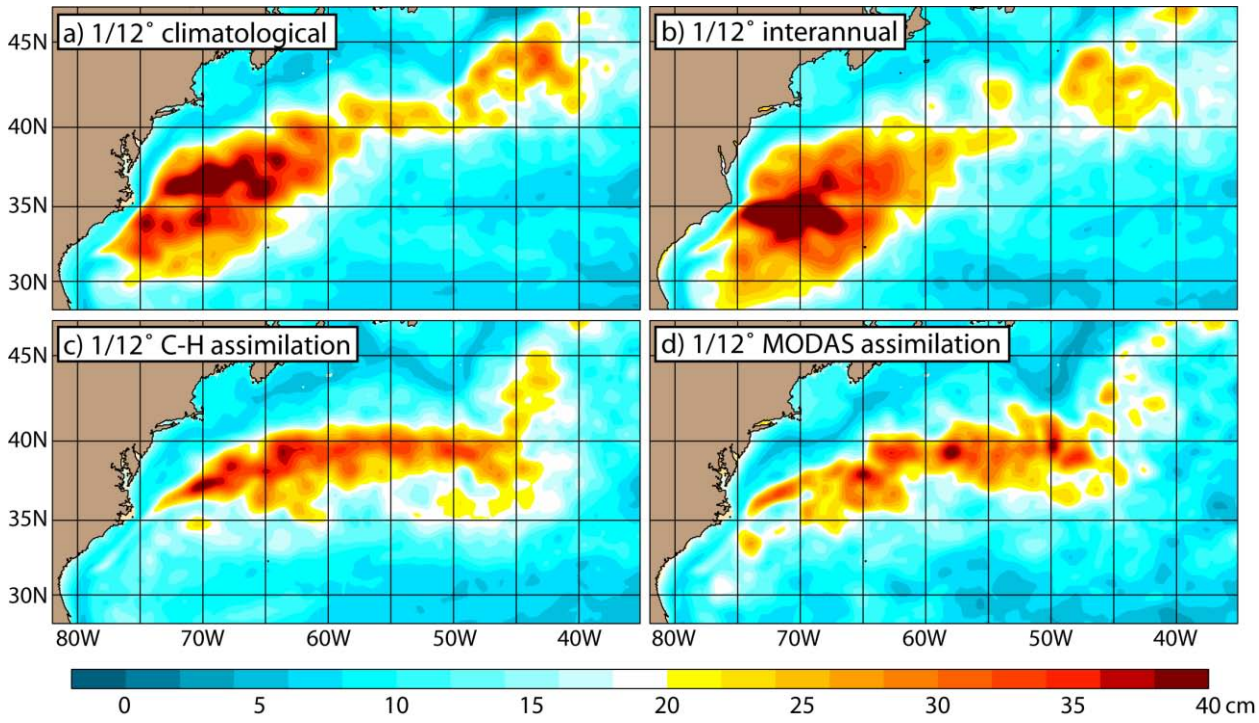

Fig. 17. Standard deviation of the sea surface height from four 1/12° global HYCOM simulations: (a) the ECMWF climatology forcing; (b) NOGAPS interannual forcing; (c) Cooper-Haines (1996) data assimilation with NOGAPS forcing and (d) MODAS synthetic temperature and salinity profile data assimilation with NOGAPS forcing.

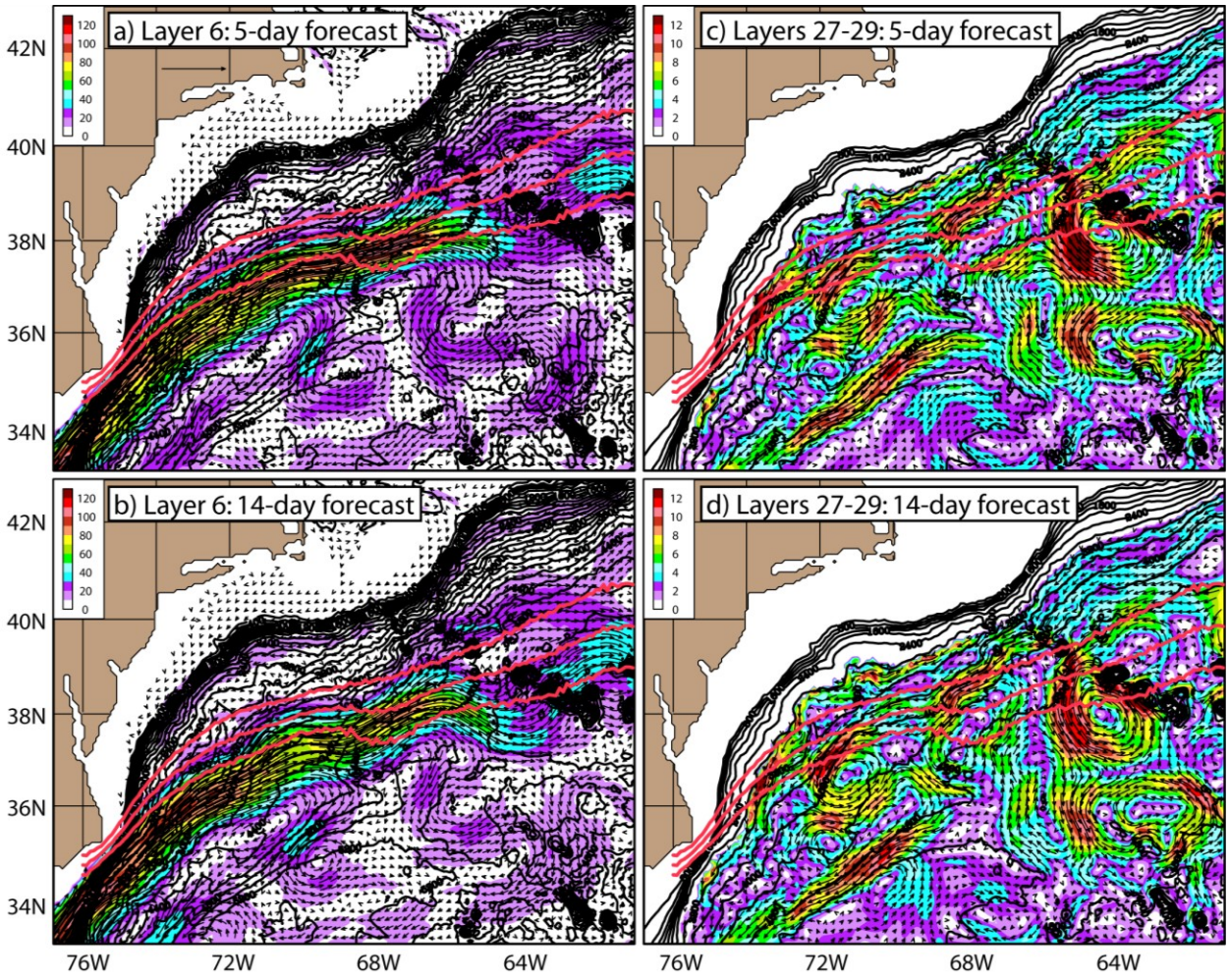

Fig. 18. The mean velocities for the forecasts starting from the state estimates of the MODAS data assimilation with the layer 6 (~25 m) velocities for the (a) 5-day forecast and the (b) 14-day forecast and the layer 27 to 29 (below approximately 3000m depth) velocities for the (c) 5-day forecast and the (d) 14-day forecast. The 15-year mean Gulf Stream northwall pathway ± 1σ from Cornillon and Sirkes is overlaid in red and the bathymetry is contoured at 200 m intervals.

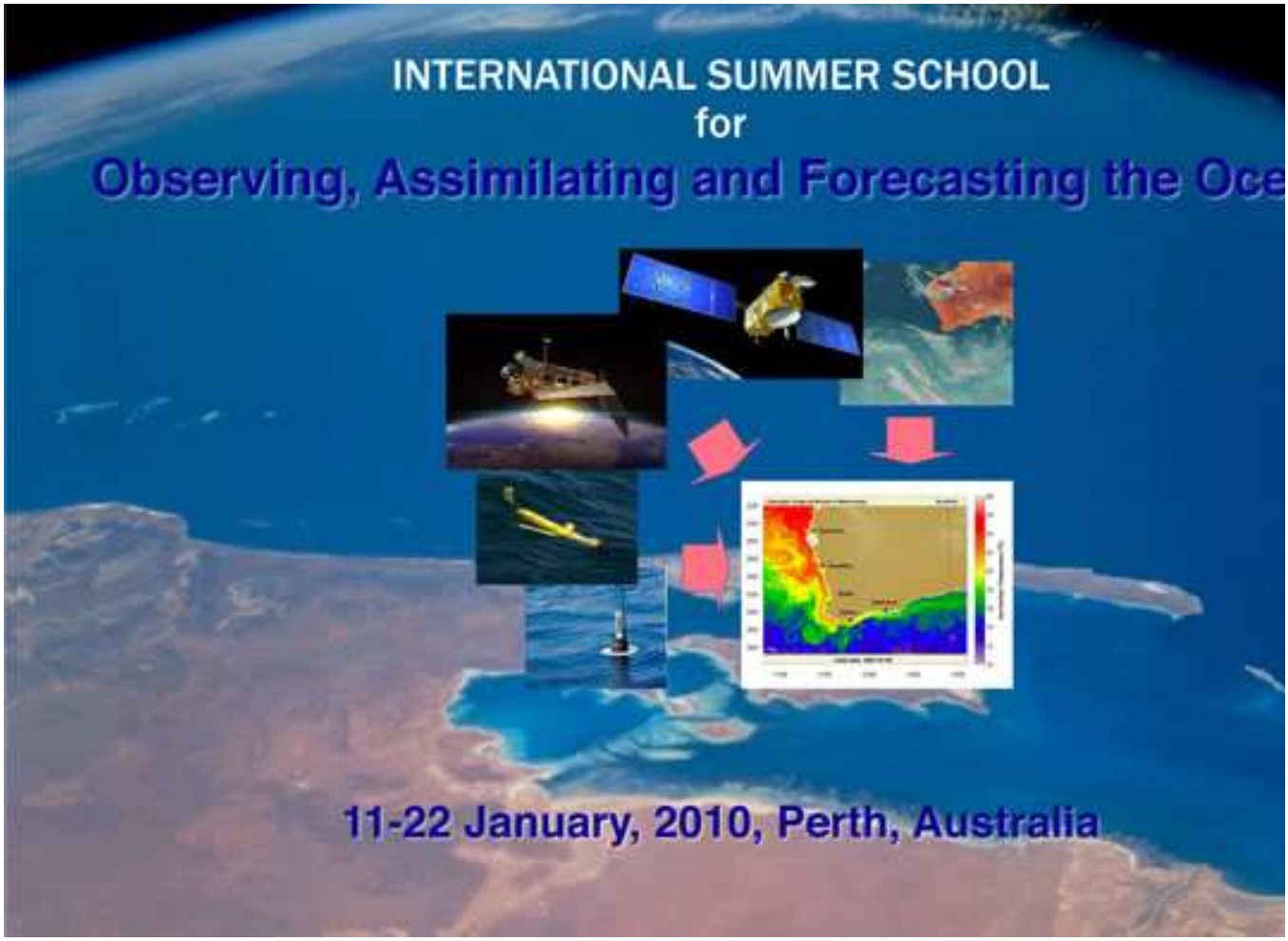

The international summer school for observing, assimilating and forecasting the ocean was a two week program offered to early career scientists, professionals and students on the current state of the art in operational oceanography and related advances in the ocean sciences.

During 11th-22nd January 2010, 66 international students came together in Perth, Western Australia to participate in the two week summer school. The students comprised participants from all inhabited continents. Australian resident students comprised 42% with good participation from Asia and Europe. The majority of Australian resident students held international passports making this summer school a truly international summer school. Only six of the students selected to attend failed to arrive in Perth. The 66 students that attended were selected from 180 applicants.

The summer school curriculum comprised of 41 lectures provided during each morning session covering all aspects of ocean forecasting and 7 computational based tutorials held in the afternoon. The lectures were provided by 28 international lecturers and covered observational oceanography, ocean modelling, ocean data assimilation, ocean forecasting and ocean applications. The computer based tutorials covered ocean modelling, ocean data assimilation, ocean data portals and servers, ocean forecast intercomparisons and paper and presentation writing.

The summer school's main objectives were:

- provide a curriculum on all aspects of ocean forecasting including observing systems, modelling, assimilation, prediction systems and applications
- attract high calibre early career professionals from throughout the world with demonstrated interests in the ocean sciences
- attract leading international professionals to provide an up to date curriculum

- provide a set of practical tutorials to reinforce theory on modelling and assimilation as well as introduce modern portals and server based technologies
- provide a positive environment and quality facilities conducive to active and effective learning and networking among participants and lecturers

The summer school on all of these objectives was a resounding success and the feedback from students and lecturers was overwhelmingly positive. This success owes a great debt of gratitude to the many contributions from many individuals. A special thank you goes to Val Jemmeson, Tim Pugh and Andy Taylor from the organising committee, to Andreas Schiller and Chari Pattiaratchi for coordination of the curriculum and local venues, Nick D'Adamo for coordination of the opening day welcome agenda and for sponsoring and coordination of two social events, Ruth Gongora-Mesas for local coordination and support, Mike Bergin for coordinating the use of a regional office vehicle in Perth. We also gratefully acknowlegde our leading sponsors Bureau of Meteorology, CSIRO, NOAA, IOC Perth Office, ArcNESS and ANNiMS.

Dr. Gary Brassington
Chair of organising committee
Centre for Australian Weather and Climate Research
Bureau of Meteorology, Melbourne, Australia

HOME
SUMMER SCHOOL REPORT
SPONSORS
CURRICULUM
LECTURERS
LECTURE PRESENTATIONS/NOTES
STUDENTS
GROUP PRESENTATIONS